

# Wave of chaos in a spatial eco-epidemiological system: Generating realistic patterns of patchiness in rabbit–lynx dynamics



Ranjit Kumar Upadhyay<sup>a,\*</sup>, Parimita Roy<sup>b</sup>, C. Venkataraman<sup>c</sup>, A. Madzvamuse<sup>d</sup>

<sup>a</sup> Department of Applied Mathematics, Indian Institute of Technology (Indian School of Mines), Dhanbad- 826 004, Jharkhand, INDIA

<sup>b</sup> School of Mathematics, Thapar University, Patiala-147004, Punjab, INDIA

<sup>c</sup> School of Mathematics and Statistics, Mathematical Institute, North Haugh, St Andrews KY16 9SS, Scotland

<sup>d</sup> Department of Mathematics, School of Mathematical and Physical Sciences, University of Sussex, Pev III, 5C15, Brighton BN19QH, United Kingdom

## ARTICLE INFO

### Article history:

Received 27 February 2016

Revised 10 July 2016

Accepted 31 August 2016

Available online 14 September 2016

### Keywords:

Eco-epidemiological model

Bifurcations analysis

Diffusion-driven instability

Turing patterns

## ABSTRACT

In the present paper, we propose and analyze an eco-epidemiological model with diffusion to study the dynamics of rabbit populations which are consumed by lynx populations. Existence, boundedness, stability and bifurcation analyses of solutions for the proposed rabbit–lynx model are performed. Results show that in the presence of diffusion the model has the potential of exhibiting Turing instability. Numerical results (finite difference and finite element methods) reveal the existence of the wave of chaos and this appears to be a dominant mode of disease dispersal. We also show the mechanism of spatiotemporal pattern formation resulting from the Hopf bifurcation analysis, which can be a potential candidate for understanding the complex spatiotemporal dynamics of eco-epidemiological systems. Implications of the asymptotic transmission rate on disease eradication among rabbit population which in turn enhances the survival of Iberian lynx are discussed.

Crown Copyright © 2016 Published by Elsevier Inc. All rights reserved.

## 1. Introduction

European rabbit and Iberian lynx are closely associated species at broad spatial and temporal scales. Both originated in the Iberian peninsula and are linked to the Mediterranean environment of south-western Europe [5,29,42]. A long term monitoring program in Spain shows a remarkable decline in rabbit numbers in 2013. A similar trend has also been observed in the main areas inhabited by Iberian lynx [15]. The Iberian lynx, a vertebrate predator, has suffered severe population reduction in the 20th century and is now on the verge of extinction [19,39]. The major decline of Iberian lynx is closely associated with sharp reduction in European rabbit (*Oryctolagus cuniculus*) abundance [44], caused by myxomatosis virus in 1950s and more recently Rabbit Hemorrhagic disease (RHD) [13,14]. European rabbit is a multifunctional species of the Iberian Mediterranean ecosystem, where it serves as prey for more than 28 predatory animals, alters the vegetation structure through seed dispersal and grazing. It also alters plant species composition, its urine have an effect on plant growth and soil fertility. It provides feeding resources for invertebrates and shelter for different species [14]. Continuous decline in biodiversity status and

an acceleration of extinction rates have occurred in recent decades, leading to a growing international commitment toward conservation [50]. As species disappear and ecosystems are destroyed, our health, peace and security, jobs and economic prosperity are also hurt and very much affected. Saving species means a better world. The number of extinction and endangered species are growing but our understanding of the causes and dynamics of the extinction is still incomplete. This study is a small step towards understanding the extinction dynamics of lynx population due to the loss of its prey rabbit population. In our study, we will consider the interaction between Iberian lynx and European rabbits as unidirectional model, because lynx are extremely rare and rabbits are abundant and widely distributed [14]. Rabbits consistently account for more than 80% of the consumed biomass in the lynx diet and hence it shows that lynx is a rabbit specialist by necessity [18]. A specialist predator dies out when its favorite food is absent or is in short supply while the generalist predator switches to an alternate food option as when it faces difficulty to find its favorite preys [51]. Therefore, the specialist predator is more prone to extinction as compared to the generalist predator. The dramatic decline in rabbit populations, caused by RHD in 1980s, had a direct impact on lynx numbers. The Iberian lynx is currently at the edge of extinction because RHDV has wiped out the rabbits on which it depends. A new variant of RHDV has been detected since 2012 in most rabbit farms and in several wild population in Spain and Por-

\* Corresponding author. Fax: +91 326 2296563.

E-mail address: [ranjit\\_ism@yahoo.com](mailto:ranjit_ism@yahoo.com) (R.K. Upadhyay).

tugal [2,12] suggesting that it has rapid spread throughout Iberian peninsula. Escaping through this extinction vortex is not possible using passive conservation measures and waiting for self recovery of populations. Recently, the issues and challenges for conserving the Iberian lynx population in Europe have been studied [46] and found that if the value of the disease transmission coefficient is reduced, the predator population (Iberian lynx) which is on the verge of extinction is saved.

In the field of eco-epidemiology, transmissible diseases are known to induce major behavioral changes in ecological systems. As a result, many models have been proposed and studied to investigate the mechanism of disease transmission [3,9,10,24–26,38,46,55]. Roy and Upadhyay [46] designed a spatial eco-epidemiological model with simple law of mass action and Holling type II functional response to understand the extinction dynamics of endangered lynx cat species. Fordham et al. [19] provided a framework for a next-generation model which simultaneously incorporates demography, dispersal, and biotic interactions into estimates of extinction risk under projected climate change. They used ecological niche models coupled to metapopulation simulations with source-sink dynamics to directly investigate the combined effects of climate change, prey availability and management intervention on the persistence of the Iberian lynx. Calvete [7] showed the impact of RHD on the dynamics of different classes of rabbit population (susceptible, infected, chronically infected and recovered class). Reddiex et al. [43] studied the impact of predation and RHD on population dynamics of rabbits. The results of such modeling efforts are helpful to predict the developmental tendencies of infectious diseases, to determine the key factors of the spread of infectious diseases and to deduce the optimum strategies for controlling and preventing the spread of diseases. Diffusion and transmission rates which are related to the reproduction rate  $R_0$ , have a great influence on the spread of the epidemics. Recent studies have shown that the incorporation of spatial structure is crucial to eco-epidemiological modeling and theory [35]. Both population and disease dynamics exhibit similar properties with regards to pattern formation in space and time. Motivated from these facts we have studied the spatiotemporal pattern formation in a lynx-rabbit eco-epidemic system.

Anderson and May [1] classified the micro-parasitic and macro-parasitic diseases into two categories that are caused by a virus or by bacteria and helminthes or arthropods, respectively. McCallum et al. [36] and Stiefsa et al. [49] suggested some form of a transmission function which is essential for designing strategy for managing disease threats to animals and human populations. Recently Delibes-Mateos [15] studied the ecosystem effects of new variant RHDV on Iberia peninsula and show how this virus could threaten the conservation of endangered predators. In this work, we propose a new eco-epidemiological model considering disease in prey population (rabbit), which is consumed by predator population (Iberian lynx) and discuss the role of asymptotic transmission rate in the context of eco-epidemiology. Eco-epidemic research deals with diseases that spreads among interacting population, where epidemic and demographic aspects are merged together in one model. Apart from considering a different transmission function, we have included spatial variations while constructing the model. Spatial component of ecological interactions has been identified as an important factor of how the ecological communities are shaped. Very little attention has been paid so far to study the spatial three species eco-epidemiological model. Eco-epidemiological modeling using reaction-diffusion models can help us to understand the distribution of species in both space and time. The main objective of this paper is to study the bidirectional spread of epidemics through the wave of chaos phenomenon as well as studying the spatiotemporal epidemic dynamics. We also underpin the parameters that have important contributions to the dynamics and pattern forma-

tion of a realistic diffusive eco-epidemiological system. We also try to understand the spatial distribution of Iberian lynx population affected by deadly rabbit disease in prey population. We emphasize that the force of infection has an important contribution to the dynamics of this designed eco-epidemiological system. In this paper, we explore the value for predator conservation by addressing the bio-geographical relationship between a species of great conservation concern, the Iberian lynx, and its staple prey, the European rabbit. We have also tried to find major issues that can guide conservation action, and prioritize conservation-oriented research lines for the future.

Hence, the structure of this paper is as follows. In Section 2, we introduce the model system and its development. In Section 3.1, we present the detailed analysis of the non-spatial eco-epidemiological model. In this section, we study the boundedness of its solutions and characterize the equilibrium states thereby obtaining conditions under which the equilibrium states exist and are locally stable. It also contains the global stability and bifurcation analysis for the non-spatial model system. In Section 4, the conditions for diffusion-driven instability for the spatiotemporal model are derived and discussed. In Section 5, we present numerical simulation results in support of the theoretical findings in 1- and 2-dimensions. We conclude and discuss the results of our studies in Section 6. It is in this section that we interpret the ecological implications of our findings.

## 2. Model development: the eco-epidemiological system

In this paper, we design an eco-epidemiological model consisting of two populations:

1. The prey population, European rabbit, whose population density is denoted by  $N$ , the number of rabbit per unit designated area.
2. The predator population, Iberian lynx, whose population density is denoted by  $P$ , the number of lynx per unit designated area.

The following assumptions are made for formulating the basic differential equations:

**Assumption 1.** In the absence of the infective ( $I(t)$ ) and predation ( $P(t)$ ), the rabbit population grows according to a logistic law with intrinsic growth rate  $r \in \mathbb{R}^+$  and carrying capacity  $K \in \mathbb{R}^+$  such that  $\frac{dN}{dt} = rN(1 - \frac{N}{K})$ .

**Assumption 2.** In the presence of Infection, the total rabbit population is divided into two classes namely, susceptible rabbit population, denoted by  $S$ , and infected rabbit population, denoted by  $I$ . Therefore, at any time  $t$ , the total prey (i.e., rabbit) density is  $N(t) = S(t) + I(t)$  which is not constant but varies according to some growth law. For simplicity, we assume that the birth and death rate depends on the population size i.e.,  $b(N) = rN$  and  $d(N) = \frac{rN^2}{K}$  respectively and have logistic form [6]. Then the total population size satisfies the logistic differential equation  $\frac{dN}{dt} = b(N) - d(N) = rN - \frac{rN^2}{K} = rN(1 - \frac{N}{K})$ , where  $K > 0$  is the carrying capacity.

**Assumption 3.** In the absence of the predator population and in the presence of the infective rabbit population, the susceptible population suffers from disease transmission, asymptotically with infection rate  $\phi = \frac{\beta S}{S+I+c}$  [17]. The infection rate represents a function of the number of infective present at a given point in time.  $\beta$  is known as the contact rate or force of infection. This signifies that the number of contacts an individual carrying a virus can have with other individuals reaches some finite maximum value due to the spatial or social distribution of the population and/or limitation of time [17].  $c$  represents half saturation constant (see

the derivation of a Holling type II functional response in prey-predator models). Biologically this constant lowers the infection rate due to spatial or social distribution and limitation of time. We assume that disease spreads among the prey only. Up to 90% of affected rabbits may die from the disease which progresses rapidly (death occurs approximately 1–3 days after infection (<http://www.peteducation.com/article.cfm?c=18+1803&aid=1625>)). Therefore we have considered no birth terms from  $I$  class. A typical  $SI$  model with an open system of variable size can be written as:

$$\begin{aligned} \frac{dS}{dt} &= \frac{S}{N}(b(N) - d(N)) - \frac{\beta SI}{N+c} = rS\left(1 - \frac{S+I}{K}\right) - \frac{\beta SI}{S+I+c} \\ &= F(S, I), \quad \frac{dI}{dt} = \frac{\beta SI}{S+I+c} - aI = G(S, I), \end{aligned} \quad (2.1)$$

where  $b, d: [0, \infty) \rightarrow (0, \infty)$  are continuously differentiable functions. In this case, when  $P = 0$ , no predation, the total rabbit population will satisfy the equation  $\frac{dN}{dt} = rS(1 - \frac{S+I}{K}) - aI$ , where  $a$  denotes the total death rate of the infected population due to disease-induced mortality and also due to natural death. The infected rabbits die after catching the infection and before they can reproduce as it is an extremely contagious and often fatal viral. Almost all adult die due to this disease while some young rabbits less than eight weeks old are less likely to become ill or die which are not capable of reproduction [54]. Therefore, we considered that only  $S$  contributes to the net linear growth of the population.

**Assumption 4.** It is assumed that predators are not smart enough to distinguish between infected and susceptible rabbits, so that predator consumes the prey species (susceptible as well as infected) according to the Holling type II functional response [4]. If predators feed upon both susceptible rabbit ( $S$ ) and infected rabbit ( $I$ ) of a single species, then selectivity or preference of the predators to susceptible and infected preys plays significant role in the system dynamics [21]. In this case traditional type II functional response should be replaced by multiple-prey type II, which can be mathematically represented by  $\omega_1 S/(S + b_1 I + c_1)$  and  $\omega_2 S/(S + b_1 I + c_1)$  for susceptible and infected rabbits, respectively [3,8,11]. The parameter  $b_1$  measures the selectivity/preference of the predator to infected rabbit over the susceptible one or vice-versa. If  $b_1 > 1$ , then predators prefer infected preys.  $b_1 = 1$  implies equal preference to susceptible and infected preys and  $0 < b_1 < 1$  means that predator prefer susceptible preys. However, in the absence of prey, the predator population die out exponentially. Assuming that predators (lynx) feed upon both the susceptible and infected preys with some preference to infected over the susceptible or vice-versa, and combining this with the systems (2.1), we formulate the required model given in (2.2). The model is basically a combination of  $SI$  model and Rosenzweig-MacArthur type predator-prey model

$$\begin{cases} \frac{dS}{dt} = rS\left(1 - \frac{S+I}{K}\right) - \frac{\beta SI}{S+I+c} - \frac{\omega_1 SP}{S+b_1 I+c_1} := Sg_1(S, I, P), \\ \frac{dI}{dt} = \frac{\beta SI}{S+I+c} - \frac{\omega_2 IP}{S+b_1 I+c_1} - aI := Ig_2(S, I, P), \\ \frac{dP}{dt} = \frac{\omega_3 IP}{S+b_1 I+c_1} + \frac{\omega_4 SP}{S+b_1 I+c_1} - \delta P := Pg_3(S, I, P), \end{cases} \quad (2.2)$$

with initial conditions  $S(0) > 0$ ,  $I(0) > 0$  and  $P(0) > 0$ . The interaction functions  $g_i$  ( $i = 1, 2, 3$ ) of the model system (2.2) are continuous and have continuous partial derivatives on  $\mathbb{R}_+^3 := \{(S, I, P) \in \mathbb{R}^3 : S(0) > 0, I(0) > 0, P(0) > 0\}$ .

All the model parameters  $r, K, \beta, c, c_1, b_1, \omega_1, \omega_2, \omega_3, \omega_4, a$  and  $\delta$  are positive constants. The infected class also suffers loss through disease induced mortality apart from its natural death. Virus transmission causes loss of susceptible ( $S$ ) and gain in infected ( $I$ ) pop-

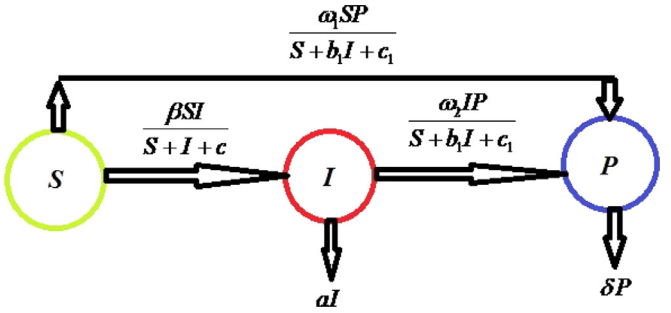


Fig. 1. Schematic diagram for the eco-epidemic model (2.2).

ulation (see Fig. 1). A brief description about variables and parameters used in the model system (2.2) is presented below in Table 1.

To proceed, we next introduce spatial variations to the model system (2.2). We assume that both prey and predator populations perform active movement in  $x$  and  $y$  directions which has been ignored in previous studies and is biologically relevant. Random movement of animals occurs because of various requirements like, search for better food, better opportunity for social interactions such as finding mates, etc. [37]. Food availability and living conditions demand that these animals migrate to other spatial locations. In the proposed model, we have included diffusion terms to model the fact that the animal movements are random and uniformly distributed in all directions. We also assume that the three species diffuse with constant diffusion rates  $D_S$ ,  $D_I$  and  $D_P$ , respectively. Furthermore, we assume that the infected rabbits diffuse at different rates to susceptible rabbit because they are weakened by disease and will have low diffusion coefficients. In our modeling, we have not considered the strong long range effect of predator and its movement in preferred directions along high rabbit concentration where the diffusion is no longer constant. If the predator and prey are confined to a fixed bounded domain  $\Omega$  in  $\mathbb{R}^2$ , we led to consider the following reaction-diffusion system:

$$\begin{cases} \frac{\partial S}{\partial t} - D_S \nabla^2 S = Sg_1(S, I, P), & z \in \Omega, t > 0, \\ \frac{\partial I}{\partial t} - D_I \nabla^2 I = Ig_2(S, I, P), & z \in \Omega, t > 0, \\ \frac{\partial P}{\partial t} - D_P \nabla^2 P = Pg_3(S, I, P), & z \in \Omega, t > 0, \end{cases} \quad (2.3)$$

with boundary conditions

$$(\mathbf{n} \cdot \nabla)S = (\mathbf{n} \cdot \nabla)I = (\mathbf{n} \cdot \nabla)P = 0, \quad \text{for } z \in \partial\Omega, t > 0, \quad (2.4)$$

and initial conditions

$$\begin{cases} S(z, 0) = S(0) > 0, \\ I(z, 0) = I(0) > 0, \\ P(z, 0) = P(0) > 0, \end{cases} \quad (2.5)$$

where  $z = (x, y) \in \Omega = [0, L] \times [0, L]$  and the kinetic functions  $g_i(S, I, P)$ ,  $i = 1, 2, 3$  are defined in (2.2). In the above, the vector  $\mathbf{n}$  is an outward unit normal vector to the boundary  $\partial\Omega$  of the habitat  $\Omega$  and the homogeneous Neumann boundary conditions are considered. The homogeneous Neumann boundary conditions signify that the system is self-contained and there is no population flux across the boundary  $\partial\Omega$ .

### 3. Analysis of the eco-epidemiological model

#### 3.1. Analysis of non-spatial model system

It is necessary to investigate the temporal dynamics of the model system (2.2) before studying the spatiotemporal model system (2.3)–(2.5).

**Table 1**  
Model parameter values and their biological meanings.

Variable/parameter	Units	Description
$S$	Prey per unit area	Susceptible rabbit population
$I$	Prey per unit area	Infected rabbit population
$P$	Predator per unit area	Predator Iberian lynx population
$r$	Per day	Intrinsic growth rate constant of susceptible rabbit population
$K$	Prey per unit area	Environmental carrying capacity
$\beta$	Per day	Contact rate
$\omega_1$	Prey per predator per day	Maximum predation rate/search rate of the susceptible rabbit population
$\omega_4$	Per day	Conversion rate of susceptible prey to predator population
$c$	Prey per unit area	Half saturation constant which lowers the infection rate due to spatial or social distribution and limitation of time.
$c_1$	Prey per unit area	Represents the half saturation constant that measures the extent to which the environment provides protection to susceptible and infected rabbit population.
$b_1$	Dimensionless	Vulnerability of infected rabbit relative to susceptible rabbit
$\omega_2$	Prey per predator per day	Maximum predation rate of the infected rabbit population
$\omega_3$	Per day	Conversion rate of the infected rabbit population to predator population
$a$	Per day	Total death rate of the infected rabbit population from causes other than predation
$\delta$	Per day	Total death rate of Iberian lynx population

### 3.1.1. Boundedness of the system

The importance of boundedness in eco-epidemic system is not only interesting for mathematical reasons but also important from an ecological point of view. This result implies that none of the interacting species grow abruptly or exponentially for a long-time interval. The number/abundance of each species is bounded due to limited resources. We will now show that system (2.2) is uniformly bounded.

**Theorem 3.1.** If the following condition

$$\omega_2\omega_4 - \omega_1\omega_3 \geq 0 \quad (3.1)$$

holds, all the non-negative solutions of model system (2.2) that start in  $\mathbb{R}_+^3$  are uniformly bounded.

**Proof.** We define a function

$$h(t) = S(t) + I(t) + \frac{\omega_1}{\omega_4}P(t). \quad (3.2)$$

Then the time-derivative of  $h(t)$  along the solutions of (2.2) is given by

$$\frac{dh}{dt} = \frac{dS}{dt} + \frac{dI}{dt} + \frac{\omega_1}{\omega_4} \frac{dP}{dt}. \quad (3.3)$$

Now for each  $\eta > 0$ , by substituting  $S(t)$  and  $I(t)$  into Eqs. (3.2) and (3.3) we obtain

$$\begin{aligned} \frac{dh}{dt} + \eta h &= S\left[\eta + r\left(1 - \frac{S}{K}\right)\right] - \left(\omega_2 - \omega_3 \frac{\omega_1}{\omega_4}\right) \frac{IP}{S + b_1 I + c_1} \\ &\quad - \frac{rSI}{K} - (a - \eta)I - \frac{\omega_1}{\omega_4}(\delta - \eta)P. \end{aligned} \quad (3.4)$$

Hence, it is easy to verify that under condition (3.1) we obtain

$$\begin{aligned} \frac{dh}{dt} + \eta h &\leq S\left[\eta + r\left(1 - \frac{S}{K}\right)\right] - (a - \eta)I - \frac{\omega_1}{\omega_4}(\delta - \eta)P \\ &\leq \frac{K(r + \eta)^2}{4r} - (a - \eta)I - \frac{\omega_1}{\omega_4}(\delta - \eta)P. \end{aligned} \quad (3.5)$$

Now defining  $\eta < \min(a, \delta)$ , then the right-hand side of the above inequality is bounded by  $\frac{K(r + \eta)^2}{4r}$ . We can thus find  $\phi > 0$  such that  $\frac{dh}{dt} + \eta h \leq \phi$ , which implies that

$$h(t) \leq e^{-\eta t}h(0) + \frac{\phi}{\eta}(1 - e^{-\eta t}) \leq \max\left(h(0), \frac{\phi}{\eta}\right). \quad (3.6)$$

Moreover, for a suitable  $M$  independent of the initial conditions, we have  $\lim_{t \rightarrow \infty} \sup h(t) \leq \frac{\phi}{\eta} = M$ . Thus,  $h(t) = S(t) + I(t) + \frac{\omega_1}{\omega_4}P(t) \leq M$ , hence all the species are uniformly bounded for any initial value in  $\mathbb{R}_+^3 = \{(S, I, P) : 0 < S \leq \eta_1, 0 < I \leq \eta_1, 0 < P \leq \eta_3\}$ .  $\square$

### 3.2. Linear stability analysis

In order to investigate the linear stability of the equilibrium points of system (2.2), first, we consider that system (2.2) can be separated into two independent subsystems. The first system is obtained by assuming the absence of the predators and can be written in the following form

$$\frac{dS}{dt} = rS\left(1 - \frac{S}{K}\right) - \frac{\beta SI}{S + I + c} = Sg_{11}(S, I), \quad (3.7)$$

$$\frac{dI}{dt} = \frac{\beta SI}{S + I + c} - aI = Ig_{12}(S, I). \quad (3.8)$$

The second subsystem is obtained in the absence of the infected prey and takes the form

$$\frac{dS}{dt} = rS\left(1 - \frac{S}{K}\right) - \frac{\omega_1 SP}{S + c_1} := Sg_{13}(S, P), \quad (3.9)$$

$$\frac{dP}{dt} = \frac{\omega_4 SP}{S + c_1} - \delta P := Pg_{14}(S, P). \quad (3.10)$$

Clearly, the interaction functions of systems (3.7)–(3.10) are continuous and have continuous partial derivatives on the state space  $\mathbb{R}^+$ . All the solutions of systems (3.7)–(3.10) which initiate in a nonnegative domain are uniformly bounded as shown in Theorem 3.1.

It is well known that the Kolmogorov theorem is applicable to a two component dynamical system and guarantees the existence of either a stable equilibrium point or a stable limit cycle behavior in the positive quadrant of the phase space of the system provided certain conditions are satisfied [51]. The amplitude and the period of the stable limit cycle oscillation depend on the values of the system parameters and strongly suggest that those natural systems which seem to exhibit a persistent pattern of reasonably regular oscillations possess a stable limit cycle [31]. When the Kolmogorov conditions are violated; one gets a repeller in the phase space.

Now we observe that the subsystem (3.7) and (3.8) is a Kolmogorov system under the condition

$$R_{01} = \frac{\beta K}{a(K + c)} > 1, \quad (3.11)$$

and the subsystem (3.9) and (3.10) is a Kolmogorov system under the condition

$$R_{02} = \frac{\omega_4 K}{\delta(K + c_1)} > 1. \quad (3.12)$$

From now on, we assume that subsystem (3.7) and (3.8) satisfies condition (3.11) and subsystem (3.9) and (3.10) satisfies condition (3.12). By applying the local stability analysis to the Kolmogorov systems (3.7)–(3.10) the following results are obtained.

### 3.2.1. Uniform steady states for the reduced two component systems

Let us consider the *SI* system given by (3.7) and (3.8). The first subsystem (3.7) and (3.8) has three nonnegative uniform steady states. The trivial uniform steady state is given by  $\bar{E}_{11} = (0, 0)$ . The disease-free equilibrium can be shown to be given by  $\bar{E}_{12} = (K, 0)$ . The nontrivial equilibrium  $\bar{E}_{13} = (\bar{S}, \bar{I})$  which exists if and only if there is a positive solution to the following set of equations

$$r\left(1 - \frac{\bar{S} + \bar{I}}{K}\right) - \frac{\beta\bar{I}}{\bar{S} + \bar{I} + c} = 0 = \frac{\beta\bar{S}}{\bar{S} + \bar{I} + c} - a. \quad (3.13)$$

Solving the above system results in

$$\bar{S} = \frac{a(-\sqrt{(a-\beta)^2B} + (a-\beta)(cr+K(a-\beta+r)))}{2(a-\beta)\beta r}, \quad (3.14)$$

$$\bar{I} = \frac{-(a-\beta)^2 K - (\beta(c-K) + a(c+K))r + (a-\beta)\sqrt{B}}{2\beta r}, \quad (3.15)$$

where

$$B = ((a-\beta)^2K^2 + 2K(\beta(c-K) + a(c+K))r + (c+K)^2r^2).$$

**Case 1:** When  $a - \beta > 0$ , then

$$\bar{S} = \frac{a(-\sqrt{B} + (cr+K(a-\beta+r)))}{2\beta r}, \quad (3.16)$$

$$\bar{I} = \frac{-(a-\beta)^2 K - (\beta(c-K) + a(c+K))r + (a-\beta)\sqrt{B}}{2\beta r}. \quad (3.17)$$

The equilibrium point  $\bar{E}_{13} = (\bar{S}, \bar{I})$  does not exist since there is no valid condition such that  $\bar{S}$  becomes positive.

**Case 2:** When  $a - \beta < 0$ , then

$$\bar{S} = \frac{a(\sqrt{B} + (cr+K(a-\beta+r)))}{2\beta r}, \quad (3.18)$$

$$\bar{I} = \frac{-(a-\beta)^2 K - (\beta(c-K) + a(c+K))r + (a-\beta)\sqrt{B}}{2\beta r}. \quad (3.19)$$

The existence criterion of the steady state population demands that  $R_{01} = \frac{\beta K}{a(K+c)} > 1$ .

Similarly, the uniform steady states corresponding to the *SP* subsystem (3.9) and (3.10) are given by  $\hat{E}_{21} = (0, 0)$ ,  $\hat{E}_{22} = (K, 0)$ , and  $\hat{E}_{23} = (\hat{S}, \hat{P})$ , where

$$\begin{aligned} \hat{S} &= \frac{c_1\delta}{\omega_4 - \delta} \quad \text{and} \\ \hat{P} &= \frac{r\omega_4 c_1 (K\omega_4 - \delta(c_1 + K))}{K\omega_1(\delta - \omega_4)^2} = \frac{r}{K\omega_1} (K - \hat{S})(\hat{S} + c_1). \end{aligned} \quad (3.20)$$

Clearly,  $\hat{E}_{23} = (\hat{S}, \hat{P})$  exists in the interior of the positive quadrant of the *SP*-plane provided the following conditions are satisfied if  $\omega_4 > \delta$  and  $R_{02} = \frac{K\omega_4}{(c_1+K)\delta} > 1$ .

### 3.2.2. Linear stability analysis of the non-spatial two component *SI* system

First, we study the local stability of the subsystem (3.7) and (3.8). The trivial equilibrium point  $\bar{E}_{11} = (0, 0)$  always exists. For  $\bar{E}_{11} = (0, 0)$ , the eigenvalues are given by  $\lambda_1 = r > 0$  and  $\lambda_2 = -a < 0$ . There is an unstable manifold along the *S*-direction and a stable manifold along the *I*-direction. Therefore, the equilibrium point  $\bar{E}_{11}$  is a saddle point. The disease-free equilibrium point  $\bar{E}_{12} = (K, 0)$  exists on the boundary of the first octant. For  $\bar{E}_{12}$ , the eigenvalues are given by  $\lambda_1 = -r < 0$  and  $\lambda_2 = \frac{\beta K - a}{K + c} < 0$  if and only if  $\beta K < a$ . Therefore the equilibrium point  $\bar{E}_{12}$  is locally asymptotically stable provided  $\beta K < a$ , otherwise, it is a saddle point.

Let us consider the stability of the nontrivial equilibrium  $\bar{E}_{13} = (\bar{S}, \bar{I})$ . The variational matrix around the endemic equilibrium point

$\bar{E}_{13}$  is given by

$$\mathbf{J}^* = \begin{bmatrix} J_{11}^* & J_{12}^* \\ J_{21}^* & J_{22}^* \end{bmatrix}$$

where

$$J_{11}^* = r\left(1 - \frac{\bar{S} + \bar{I}}{K}\right) - \frac{r\bar{S}}{K} - \frac{\beta\bar{I}(c + \bar{I})}{(c + \bar{I} + \bar{S})^2}, \quad J_{12}^* = -\frac{r\bar{S}}{K} - \frac{\beta\bar{S}(c + \bar{S})}{(c + \bar{I} + \bar{S})^2},$$

$$J_{21}^* = \frac{\beta\bar{I}(c + \bar{I})}{(c + \bar{I} + \bar{S})^2}, \quad J_{22}^* = -a + \frac{\beta\bar{S}(c + \bar{S})}{(c + \bar{I} + \bar{S})^2},$$

and

$$\text{Tr}(\mathbf{J}) = (J_{11}^* + J_{22}^*) = -a - \frac{r\bar{S}}{K} + \frac{\beta(\bar{S} - \bar{I})}{c + \bar{I} + \bar{S}} + r\left(1 - \frac{\bar{S} + \bar{I}}{K}\right),$$

$$\text{Det}(\mathbf{J}) = J_{11}^* J_{22}^* - J_{21}^* J_{12}^* = \frac{\beta r \bar{S} (\bar{I}^2 - \bar{I}\bar{S} + (K - 2\bar{S})(c + \bar{S})) + a(\beta\bar{I}(c + \bar{I})K + r(c + \bar{I} + \bar{S})^2(\bar{I} - K + 2\bar{S}))}{K(c + \bar{I} + \bar{S})^2}.$$

If  $\bar{E}_{13} = (\bar{S}, \bar{I})$  exists, i.e. if  $R_{01} = \frac{\beta K}{a(K+c)} > 1$  holds, then the eigenvalues of  $\mathbf{J}$  have negative real parts and hence the equilibrium point  $\bar{E}_{13}$  is stable.

**Lemma 3.1.** *The equilibrium point  $\bar{E}_{13} = (\bar{S}, \bar{I})$  is locally asymptotically stable in the interior of the *SI*-plane whenever it exists.*

### 3.2.3. Linear stability analysis of the non-spatial two component *SP* system

Similarly, the stability of the second subsystem (3.9) and (3.10) can be carried out as follows. The variational matrices of the subsystem (3.9) and (3.10) at  $\hat{E}_{21}$  and  $\hat{E}_{22}$  can be written as

$$\mathbf{J}|_{\hat{E}_{21}} = \begin{bmatrix} r & 0 \\ 0 & -\delta \end{bmatrix} \quad \text{and} \quad \mathbf{J}|_{\hat{E}_{22}} = \begin{bmatrix} -r & -\frac{K\omega_1}{c_1+K} \\ 0 & -\delta + \frac{K\omega_4}{c_1+K} \end{bmatrix}.$$

Clearly  $\hat{E}_{21}$  is a saddle point since  $r > 0$  and  $-\delta < 0$ . Hence there is a locally stable manifold in the *P*-direction and with a locally unstable manifold in the *S*-direction. Similarly, the eigenvalues of  $\hat{E}_{22}$  are  $-r < 0$  and  $-\delta + \frac{K\omega_4}{c_1+K} < 0$ . So,  $\hat{E}_{22}$  is locally asymptotically stable if and only if  $\frac{K\omega_4}{c_1+K} < \delta$ . Finally, the variational matrix of the subsystem (3.9) and (3.10) at the positive equilibrium point  $\hat{E}_{23}$  can be written in the form

$$\mathbf{J}|_{\hat{E}_{23}} = \begin{bmatrix} J_{11} & J_{12} \\ J_{21} & J_{22} \end{bmatrix},$$

where

$$\begin{cases} J_{11} = \frac{\delta r}{\omega_4} \left(1 - \frac{c_1}{K} \left(\frac{\omega_4 + \delta}{\omega_4 - \delta}\right)\right), & J_{12} = -\frac{\delta\omega_1}{\omega_4}, \\ J_{21} = \frac{-\delta(c_1 + K)r + Kr\omega_4}{K\omega_1}, & \text{and} \quad J_{22} = 0. \end{cases}$$

Therefore, it is easy to verify that the eigenvalues of  $\mathbf{J}$  satisfy the relations

$$\begin{aligned} \hat{\lambda}_1 + \hat{\lambda}_2 &= \frac{\delta r}{\omega_4} \left(1 - \frac{c_1}{K} \left(\frac{\omega_4 + \delta}{\omega_4 - \delta}\right)\right), \quad \text{and} \\ \hat{\lambda}_1 \hat{\lambda}_2 &= \frac{\delta r}{\omega_4} \left(\frac{-\delta(c_1 + K) + Kr\omega_4}{K}\right). \end{aligned} \quad (3.21)$$

Thus, if

$$\frac{K}{c_1} < \frac{\omega_4 + \delta}{\omega_4 - \delta}, \quad (3.22)$$

holds then both eigenvalues have negative real parts and hence  $\hat{E}_{23}$  is locally asymptotically stable in the interior of the positive quadrant of the *SP*-plane, otherwise its an unstable point.

### 3.2.4. Uniform steady states for the three component non-spatial SIP system

In this section, the existence of the equilibrium points and local stability of the model system (2.2) are discussed. The system has five possible non-negative equilibrium points. The trivial equilibrium point  $E_0 = (0, 0, 0)$  always exists. The equilibrium point  $E_1 = (K, 0, 0)$  exists on the boundary of the first octant. The predator-free equilibrium point  $E_2 = (\bar{S}, \bar{I}, 0)$ , where  $\bar{S}$  and  $\bar{I}$  are given by Eqs. (3.18) and (3.19), exists provided  $R_{01} = \frac{\beta K}{a(K+c)} > 1$ . The disease-free equilibrium point  $E_3 = (\hat{S}, 0, \hat{P})$ , where  $\hat{S}$  and  $\hat{P}$  are given by (3.20), exists provided the condition (3.12) is satisfied. The non-trivial equilibrium  $(S^*, I^*, P^*)$  exists if and only if there is a positive solution to the following set of equations

$$g_1(S, I, P) = r\left(1 - \frac{S+I}{K}\right) - \frac{\beta I}{S+I+c} - \frac{\omega_1 P}{S+b_1 I+c_1} = 0, \quad (3.23)$$

$$g_2(S, I, P) = \frac{\beta S}{S+I+c} - \frac{\omega_2 P}{S+b_1 I+c_1} - a = 0, \quad (3.24)$$

$$g_3(S, I, P) = \frac{\omega_3 I}{S+b_1 I+c_1} + \frac{\omega_4 S}{S+b_1 I+c_1} - \delta = 0. \quad (3.25)$$

Now, from Eq. (3.24), solving for  $P$  we have

$$P = \frac{(c_1 + b_1 I + S)(\beta S - a(c + I + S))}{(c + I + S)\omega_2}. \quad (3.26)$$

Substituting Eq. (3.26) into Eq. (3.23) and simplifying Eq. (3.25), we obtain the following system of nonlinear algebraic equations

$$\begin{aligned} f(S, I) &= K(a(c + I + S) - S\beta)\omega_1 \\ &\quad - (r(c + I + S)(I - k + S) + IK\beta)\omega_2 = 0, \end{aligned} \quad (3.27)$$

$$g(S, I) = (c_1 + b_1 I + S)\delta - S\omega_4 - I\omega_3 = 0. \quad (3.28)$$

From Eq. (3.27) we note the following: when  $I(t) \rightarrow 0$  then  $S(t) \rightarrow S_a$  as  $t \rightarrow \infty$ , where  $S_a$  is the positive root of the quadratic polynomial

$$p_2 S^2 + p_1 S + p_0 = 0, \quad (3.29)$$

with coefficients

$$\begin{aligned} p_0 &= cK(a\omega_1 + r\omega_2) > 0, \quad p_1 = K(a - \beta)\omega_1 + (-c + K)r\omega_2, \\ p_2 &= -r\omega_2 < 0. \end{aligned}$$

This implies that there is exactly one positive root for the quadratic equation (3.29) irrespective of the sign of  $p_1$ . From Eq. (3.27) we have that

$$\frac{dS}{dI} = -\frac{\frac{\partial f}{\partial I}}{\frac{\partial g}{\partial S}} = \frac{A_1}{B_1}, \quad (3.30)$$

where

$$A_1 = -aK\omega_1 + (r(c + 2I - K + 2S) + K\beta)\omega_2, \quad (3.31)$$

$$B_1 = K(a - \beta)\omega_1 - r\omega_2(c + 2I - K + 2S). \quad (3.32)$$

It is clear that

$$\frac{dS}{dI} > 0 \text{ if either } A_1 > 0 \text{ and } B_1 > 0 \text{ or } A_1 < 0 \text{ and } B_1 < 0 \text{ holds.} \quad (3.33)$$

Also from (3.28), we note that when  $I(t) \rightarrow 0$  then  $S(t) \rightarrow S_b$  as  $t \rightarrow \infty$ , where  $S_b = \frac{c_1 \delta}{\omega_3 - \delta}$ . We note that  $S_b > 0$  if the first inequality given by  $\omega_3 > \delta$  holds. We also have

$$\frac{dS}{dI} = -\frac{\frac{\partial g}{\partial I}}{\frac{\partial g}{\partial S}} = -\frac{A_2}{B_2} \quad (3.34)$$

where

$$A_2 = b_1 \delta - \omega_3, \quad \text{and} \quad B_2 = \delta - \omega_4. \quad (3.35)$$

It follows then that

$$\frac{dS}{dI} < 0 \text{ if either } A_2 > 0 \text{ and } B_2 > 0 \text{ or } A_2 < 0 \text{ and } B_2 < 0 \text{ holds.} \quad (3.36)$$

From the above analysis we note that two isolines (3.27) and (3.28) intersect at a unique equilibrium point  $(S^*, I^*)$  if in addition to conditions (3.12), (3.33) and (3.36), the inequality  $S_a < S_b$  holds.

Knowing the values of  $S^*$  and  $I^*$ , the value of  $P^*$  can be calculated from

$$P^* = \frac{(c_1 + b_1 I^* + S^*)(\beta S^* - a(c + I^* + S^*))}{(c + I^* + S^*)\omega_2}. \quad (3.37)$$

It must be noted that for  $P^*$  to be positive, we must have  $\beta S^* > a(S^* + I^* + c)$ . This completes the existence of  $E^*(S^*, I^*, P^*)$ . From the above analysis the following proposition can be proved.

**Proposition 3.1.** *If the following conditions holds*

1.  $A_1 > 0$  and  $B_1 > 0$  or  $A_1 < 0$  and  $B_1 < 0$ .
2.  $A_2 > 0$  and  $B_2 > 0$  or  $A_2 < 0$  and  $B_2 < 0$ .
3.  $S_a < S_b$ , where  $A_1, B_1, A_2, B_2$  and  $S_a, S_b$  are defined above.

*Then the nontrivial equilibrium  $E^*(S^*, I^*, P^*)$  exists if  $(\beta - a)S^* - a(I^* + c) > 0$ .*

### 3.2.5. Linear stability analysis of the non-spatial three component SIP system

Now, in order to investigate the local behavior of the model system (2.2) around each of the equilibrium point, the variational matrix  $\mathbf{J}$  evaluated at each point  $(S, I, P)$  is computed as follows

$$\mathbf{J}(E) = \begin{bmatrix} a_{11} & a_{12} & a_{13} \\ a_{21} & a_{22} & a_{23} \\ a_{31} & a_{32} & a_{33} \end{bmatrix}.$$

The entries of the matrix are

$$\begin{aligned} a_{11} &= \frac{r(K - I - 2S)}{K} - \frac{\beta I(c + I)}{(c + I + S)^2} - \frac{\omega_1 P(c_1 + b_1 I)}{(c_1 + b_1 I + S)^2}, \\ a_{12} &= S\left(\frac{b_1 \omega_1 P}{(c_1 + b_1 I + S)^2 - \frac{r}{K} - \frac{(c+S)\beta}{(c+I+S)^2}}\right), \\ a_{13} &= -\frac{S\omega_1}{c_1 + b_1 I + S}, \quad a_{21} = I\left(\frac{\beta(c + I)}{(c + I + S)^2} + \frac{P\omega_2}{(c_1 + b_1 I + S)^2}\right), \\ a_{22} &= -a + \frac{\beta S(c + S)}{(c + I + S)^2} - \frac{\omega_2 P(c_1 + S)}{(c_1 + b_1 I + S)^2}, \quad a_{23} = -\frac{\omega_2 I}{c_1 + b_1 I + S}, \\ a_{31} &= \frac{P((c_1 + b_1 I)\omega_4 - I\omega_3)}{(c_1 + b_1 I + S)^2}, \quad a_{32} = \frac{P(-b_1 \omega_4 S + (c_1 + S)\omega_3)}{(c_1 + b_1 I + S)^2}, \\ a_{33} &= \frac{S\omega_4 + I\omega_3 - (c_1 + b_1 I + S)\delta}{c_1 + b_1 I + S}. \end{aligned}$$

We denote  $\mathbf{J}(E_k) = \mathbf{J}(E)$  valued at  $E_k$  and  $a_{ij}^{[k]} = a_{ij}$  with  $i = 1, 2, 3$ ,  $j = 1, 2, 3$  and  $k = 0, 1, 2, 3$ . Now, in order to study the local stability of system (2.2), the variational matrix of system (2.2) is computed at each of the above equilibrium points and then the eigenvalues are determined.

The variational matrix at  $E_0$  is

$$\mathbf{J}(E_0) = \begin{bmatrix} r & 0 & 0 \\ 0 & -a & 0 \\ 0 & 0 & -\delta \end{bmatrix}.$$

For  $E_0$ , the eigenvalues are  $r, -a, -\delta$ . There is an unstable manifold along the  $S$ -direction and a stable manifold along the  $IP$ -direction. Therefore, the equilibrium point  $E_0$  is a saddle point.

The variational matrix at  $E_1$  is

$$J(E_1) = \begin{bmatrix} -r & -\frac{\beta K}{c+K} - r & -\frac{K\omega_1}{c_1+K} \\ 0 & -a + \frac{\beta K}{c+K} & 0 \\ 0 & 0 & -\delta + \frac{K\omega_4}{c_1+K} \end{bmatrix}.$$

The corresponding eigenvalues are  $-a + \frac{\beta K}{c+K}$ ,  $-r$ ,  $-\delta + \frac{K\omega_4}{c_1+K}$ . Therefore, the equilibrium point  $E_1$  is locally asymptotically stable provided  $R_{01} < 1$  and  $R_{02} < 1$ . Also  $E_1$  is a saddle point if at least one of the conditions  $R_{01} > 1$  or  $R_{02} > 1$  holds.

The variational matrix at the predator-free equilibrium point  $E_2 = (\bar{S}, \bar{I}, 0)$  can be written as

$$J(E_2) = \begin{bmatrix} \frac{r(K-2\bar{S}-\bar{I})}{K} - \frac{\beta\bar{I}(c+\bar{I})}{(c+\bar{I}+\bar{S})^2} & \bar{S}\left[-\frac{r}{K} - \frac{\beta(c+\bar{S})}{(c+\bar{I}+\bar{S})^2}\right] \\ \frac{\beta\bar{I}(c+\bar{I})}{(c+\bar{I}+\bar{S})^2} & -a + \frac{\beta\bar{S}(c+\bar{S})}{(c+\bar{I}+\bar{S})^2} \\ 0 & 0 \end{bmatrix}.$$

Clearly the equilibrium point  $E_2 = (\bar{S}, \bar{I}, 0)$  has the same stability properties as  $\bar{E}_{13} = (\bar{S}, \bar{I})$  in the interior positive coordinate of the  $SI$ -plane. However, the stability of the point  $E_2 = (\bar{S}, \bar{I}, 0)$  is determined by the positive direction orthogonal to the  $SI$ -plane, i.e., the  $P$ -direction, depending on whether the eigenvalue

$$\bar{\lambda}_p = -\delta + \frac{\omega_3\bar{I} + \omega_4\bar{S}}{c_1 + \bar{S} + b_1\bar{I}} \quad (3.38)$$

is negative or positive, respectively.

According to Lemma 3.1, both eigenvalues  $\bar{\lambda}_S$  and  $\bar{\lambda}_I$  have negative real parts, while the eigenvalue  $\bar{\lambda}_P$  will be negative if and only if

$$\frac{\omega_3\bar{I} + \omega_4\bar{S}}{c_1 + \bar{S} + b_1\bar{I}} < \delta. \quad (3.39)$$

Therefore,  $E_2 = (\bar{S}, \bar{I}, 0)$  is locally asymptotically stable provided condition (3.39) holds.

The variational matrix at the disease-free equilibrium point  $E_3 = (\hat{S}, 0, \hat{P})$  is

$$J(E_3) = \begin{bmatrix} r - \frac{2r\hat{S}}{K} - \frac{c_1\omega_1\hat{P}}{(c_1+\hat{S})^2} & -\hat{S}\left(-\frac{r}{K} - \frac{\beta}{c+\hat{S}} + \frac{b_1\hat{P}\omega_1}{(c_1+\hat{S})^2}\right) & -\frac{\omega_1\hat{S}}{c_1+\hat{S}} \\ 0 & -a - \frac{\omega_2\hat{P}}{\hat{S}+c_1} + \frac{\beta\hat{S}}{c+\hat{S}} & 0 \\ \frac{\omega_4c_1\hat{P}}{(c_1+\hat{S})^2} & \frac{\hat{P}((c_1+\hat{S})\omega_3 - b_1\hat{S}\omega_4)}{(c_1+\hat{S})^2} & 0 \end{bmatrix}.$$

Then the eigenvalues of  $J(E_3)$  satisfy the relations  $\hat{\lambda}_S + \hat{\lambda}_P = \hat{\lambda}_1 + \hat{\lambda}_2$  and  $\hat{\lambda}_S\hat{\lambda}_P = \hat{\lambda}_1\hat{\lambda}_2$ , where  $\hat{\lambda}_1$  and  $\hat{\lambda}_2$  represent the eigenvalues of  $J(\hat{E}_{23})$  and satisfy (3.21). However,  $\hat{\lambda}_I = -a - \frac{\omega_2\hat{P}}{\hat{S}+c_1} + \frac{\beta\hat{S}}{c+\hat{S}}$ , where  $\hat{\lambda}_S$ ,  $\hat{\lambda}_I$  and  $\hat{\lambda}_P$  represents the eigenvalues of  $J(E_3)$  in the  $S$ ,  $I$  and  $P$  directions, respectively. Therefore, it is clear that the eigenvalues  $\hat{\lambda}_S$  and  $\hat{\lambda}_P$  have negative real parts if and only if condition (3.22) holds. However the eigenvalue  $\hat{\lambda}_I$  is negative if and only if the following condition holds, respectively

$$R_0 = \frac{\beta\hat{S}(\hat{S}+c_1)}{(a(c_1+\hat{S}) + \omega_2\hat{P})(c+\hat{S})} < 1. \quad (3.40)$$

Following Hsieh and Hsiao [28], the term  $R_0 = \frac{\beta\hat{S}(\hat{S}+c_1)}{(a(c_1+\hat{S}) + \omega_2\hat{P})(c+\hat{S})}$  gives the disease basic reproduction number of the system.  $R_0$  is defined as the expected number of offsprings a typical individual

produces in its life-time or in epizootiology, as the expected number of secondary infections produced by a single infective individual in a completely susceptible population during its entire infectious period [16]. If  $R_0 < 1$ , it implies that the infected prey will become extinct and consequently the disease will be eradicated from the system. Actually,  $R_0 < 1$  is a necessary condition for local stability of  $E_3 = (\hat{S}, 0, \hat{P})$ . Thus,  $E_3 = (\hat{S}, 0, \hat{P})$  is asymptotically stable if and only if conditions (3.22) and (3.40) hold. When  $R_0 = 1$  one of the eigenvalue of  $E_3$  becomes zero and it exhibit transcritical bifurcation (detailed analysis is given in Theorem 3.5).

**Theorem 3.2.** The constant positive steady state  $E^*(S^*, I^*, P^*)$  of system (2.2) is locally asymptotically stable provided the following conditions hold

$$\begin{bmatrix} \frac{\omega_1\bar{S}}{(c_1+\bar{S}+b_1\bar{I})} \\ \frac{\omega_2\bar{I}}{c_1+\bar{S}+b_1\bar{I}} \\ -\delta + \frac{\omega_3\bar{I} + \omega_4\bar{S}}{c_1+\bar{S}+b_1\bar{I}} \end{bmatrix}.$$

$$r \leq \frac{I^*(c+I^*)\beta}{(c+I^*+S^*)^2}, a \geq \frac{S^*(c+S^*)\beta}{(c+I^*+S^*)^2}, \quad (3.41)$$

$$b_1 < \frac{(c_1+S^*)\omega_3}{S^*\omega_4}, \frac{\omega_3}{\omega_4} \leq b_1, \quad (3.42)$$

$$P^* < \frac{(c_1+b_1I^*+S^*)^2(r(c+I^*+S^*)^2+K(c+S^*)\beta)}{b_1K(c+I^*+S^*)^2\omega_1}, \quad (3.43)$$

$$a \geq \frac{KS^*(c+S^*)\beta\omega_1 + I^*(r(c+I^*+S^*)^2+K(c+S^*)\beta)\omega_2}{K(c+I^*+S^*)^2\omega_1}, \quad (3.44)$$

$$\omega_2 \geq \omega_1, a \geq \frac{S^*\beta((c+I^*)\omega_1 + (c+S^*)\omega_2)}{(c+I^*+S^*)^2\omega_2}. \quad (3.45)$$

**Proof.** The model system (2.2) is linearized at  $E^*(S^*, I^*, P^*)$  to yield the stability matrix

$$J(E^*) = \begin{bmatrix} a_{11}^* & a_{12}^* & a_{13}^* \\ a_{21}^* & a_{22}^* & a_{23}^* \\ a_{31}^* & a_{32}^* & a_{33}^* \end{bmatrix}.$$

The entries of the matrix are

$$a_{11}^* = \frac{r(-I+K-2S^*)}{K} - \frac{I^*(c+I^*)\beta}{(c+I^*+S^*)^2} - \frac{(c_1+b_1I^*)P^*\omega_1}{(c_1+b_1I^*+S^*)^2},$$

$$a_{12}^* = S^*\left(-\frac{r}{K} - \frac{(c+S^*)\beta}{(c+I^*+S^*)^2} + \frac{b_1P^*\omega_1}{(c_1+b_1I^*+S^*)^2}\right),$$

$$a_{13}^* = -\frac{S^*\omega_1}{c_1+b_1I^*+S^*},$$

$$a_{21}^* = I^*\left(\frac{(c+I^*)\beta}{(c+I^*+S^*)^2} + \frac{P^*\omega_2}{(c_1+b_1I^*+S^*)^2}\right),$$

$$a_{22}^* = -a + \frac{S^*(c+S^*)\beta}{(c+I^*+S^*)^2} - \frac{P^*(c_1+S^*)\omega_2}{(c_1+b_1I^*+S^*)^2},$$

$$a_{23}^* = -\frac{I^*\omega_2}{c_1+b_1I^*+S^*},$$

$$a_{31}^* = \frac{P^*((c_1+b_1I^*)\omega_4 - I^*\omega_3)}{(c_1+b_1I^*+S^*)^2}, a_{32}^* = \frac{P^*(-b_1S^*\omega_4 + (c_1+S^*)\omega_3)}{(c_1+b_1I^*+S^*)^2},$$

$$a_{33} = 0.$$

The characteristics equation of  $E^*(S^*, I^*, P^*)$  is given by

$$\lambda^3 + A_1\lambda^2 + A_2\lambda + A_3 = 0, \quad (3.46)$$

where

$$A_1 = -(a_{11} + a_{22}), \quad (3.47)$$

$$A_2 = (a_{11}a_{22} - a_{12}a_{21}) - (a_{23}a_{32} + a_{13}a_{31}), \quad (3.48)$$

$$A_3 = (a_{13}a_{22} - a_{12}a_{23})a_{31} + (a_{11}a_{23} - a_{13}a_{21})a_{32}, \quad (3.49)$$

$$A_1A_2 - A_3 = A_1(a_{11}a_{22} - a_{12}a_{21}) + a_{31}(a_{11}a_{13} + a_{12}a_{23}) \\ + a_{32}(a_{22}a_{23} + a_{13}a_{21}). \quad (3.50)$$

Now according to Routh–Hurwitz criterion  $E^*$  is locally asymptotically stable if

$$A_1 > 0, \quad A_3 > 0, \quad A_1A_2 - A_3 > 0. \quad (3.51)$$

Clearly from condition (3.41) we obtain that  $a_{11} < 0$ ,  $a_{22} < 0$  and hence  $A_1 > 0$ . Now, if (3.42) and (3.43) holds  $a_{31} > 0$ ,  $a_{32} > 0$  and  $a_{12} < 0$ , therefore the second term of  $A_3$  is positive. Moreover, it is easy to verify that the first term  $A_3$  i.e.  $(a_{13}a_{22} - a_{12}a_{23})$  will be positive if condition (3.44) holds. It can be easily shown that the first and the second terms of  $A_1A_2 - A_3$  are positive. However the third term of  $A_1A_2 - A_3$  will be positive if  $(a_{22}a_{23} + a_{13}a_{21}) > 0$ , which is satisfied provided condition (3.45) holds. Hence the model system (2.2) is locally asymptotically stable under the conditions (3.41)–(3.45).  $\square$

**Example 3.1.** For the following set of biologically realistic parameter values (used in numerical simulation)  $r = 6.1$ ,  $K = 100$ ,  $\beta = 7.69$ ,  $b_1 = 3$ ,  $\omega_1 = 0.5$ ,  $c = 10$ ,  $c_1 = 48$ ,  $\omega_2 = 4.5$ ,  $a = 0.19008$ ,  $\omega_3 = 0.9$ , and  $\omega_4 = 0.12$ , and  $\delta = 0.14$  the positive equilibrium point  $E^* = (48.003797, 16.000168, 153.545549)$  settles down to an asymptotic state which is confirmed by the Routh–Hurwitz criterion ( $A_1 = 1.15116 > 0$ ,  $A_2 = 6.42556 > 0$ ,  $A_3 = 0.592248 > 0$ , and  $A_1A_2 - A_3 = 6.80459 > 0$ ).

Biologically, it means that the equilibrium  $E^*$  will act as sink and will attracts nearby solutions at  $t \rightarrow \infty$ .

### 3.3. Global stability of the SIP non-spatial model system

**Theorem 3.3.** Assuming that the positive equilibrium point  $E^* = (S^*, I^*, P^*)$  is locally asymptotically stable. Then it is a globally stable in the interior of the positive octant (i.e.,  $\text{Int } \mathbb{R}_+^3$ ) provided that

$$\frac{3r}{2K} + \frac{\beta(S^* + c)}{2(\eta_1 + \eta_2 + c)(S^* + I^* + c)} \\ > \frac{P^* \omega_1(b_1 + 2) + \omega_2 k_1}{2c_1(S^* + b_1 I^* + c_1)} + \frac{\beta I^*(k_1 + 2) + k_1 c}{2c(S^* + I^* + c)}, \quad (3.52)$$

and

$$\frac{r}{2K} + \frac{\beta(3S^* + c)}{2(\eta_1 + \eta_2 + c)(S^* + I^* + c)} \\ > \frac{\beta k_1(I^* + c)}{2c(S^* + I^* + c)} + \frac{P^*(\omega_1 b_1 + \omega_2 k_1 + 2\omega_2 b_1)}{2c_1(S^* + b_1 I^* + c_1)}. \quad (3.53)$$

where  $\eta_1$ ,  $\eta_2$  and  $\eta_3$  are defined in  $\mathbb{R}_+^3 = \{(S, I, P) : 0 < S \leq \eta_1, 0 < I \leq \eta_2, 0 < P \leq \eta_3\}$

**Proof.** Consider the following positive definite Lyapunov function about the equilibrium point

$$V(t) = \left[ S - S^* - S^* \ln \frac{S}{S^*} \right] + k_1 \left[ I - I^* - I^* \ln \frac{I^*}{I} \right] \\ + k_2 \left[ P - P^* - P^* \ln \frac{P^*}{P} \right], \quad (3.54)$$

where  $k_1$  and  $k_2$  are positive constants to be chosen suitably later on. Obviously,  $V$  is a continuous function in the interior of

$\mathbb{R}_+^3$ . Now, in order to investigate the global dynamics of the non-negative equilibrium point  $E^* = (S^*, I^*, P^*)$  of the model system, the derivative of  $V$  with respect to time along the solution of the system is computed as

$$\frac{dV}{dt} = \frac{dV_1}{dt} + \frac{dV_2}{dt} + \frac{dV_3}{dt}.$$

Simple algebraic manipulations yield

$$\left\{ \begin{aligned} \frac{dV}{dt} = & - \left( \frac{r}{K} - \frac{\beta I^*}{(S^* + I^* + c)(S + I + c)} \right. \right. \\ & \left. \left. - \frac{\omega_1 P^*}{(S + b_1 I + c_1)(S^* + b_1 I^* + c_1)} \right) (S - S^*)^2 \\ & + \left( -\frac{r}{K} - \frac{\beta((S^* + c) - k_1(I^* + c))}{(S + I + c)(S^* + I^* + c)} \right. \\ & \left. + \frac{P^*(\omega_1 b_1 + \omega_2 k_1)}{(S + b_1 I + c_1)(S^* + b_1 I^* + c_1)} \right) (S - S^*)(I - I^*) \\ & - k_1 \left( \frac{\beta S^*}{(S + I + c)(S^* + I^* + c)} \right. \\ & \left. - \frac{\omega_2 b_1 P^*}{(S^* + b_1 I^* + c_1)(S + b_1 I + c_1)} \right) (I - I^*)^2 \\ & + \left( \frac{k_2((\omega_4 b_1 - \omega_3)I^* + \omega_4 c_1) - \omega_1(S^* + b_1 I^*)}{(S^* + b_1 I^* + c_1)(S + b_1 I + c_1)} \right. \\ & \left. \times (I - I^*)(P - P^*) \right) \\ & + \left( \frac{k_2((\omega_4 b_1 - \omega_3)I^* + \omega_4 c_1) - \omega_1(S^* + b_1 I^*)}{(S^* + b_1 I^* + c_1)(S + b_1 I + c_1)} \right. \\ & \left. \times (S - S^*)(P - P^*) \right). \end{aligned} \right.$$

Choosing  $k_2 = \frac{\omega_1(S^* + b_1 I^*)}{(\omega_4 b_1 - \omega_3)I^* + \omega_4 c_1}$  and  $k_1 = \frac{k_2((S^* + c_1)\omega_3 - \omega_4 b_1 S^*)}{\omega_2(S^* + b_1 I^* + c_1)}$  we have

$$\begin{aligned} \frac{dV}{dt} \leq & - \left( \frac{r}{K} - \frac{\beta I^*}{(S^* + I^* + c)(S + I + c)} \right. \\ & \left. - \frac{\omega_1 P^*}{(S + b_1 I + c_1)(S^* + b_1 I^* + c_1)} \right) (S - S^*)^2 \\ & - k_1 \left( \frac{\beta S^*}{(S + I + c)(S^* + I^* + c)} \right. \\ & \left. - \frac{\omega_2 b_1 P^*}{(S^* + b_1 I^* + c_1)(S + b_1 I + c_1)} \right) (I - I^*)^2 \\ & + \left( -\frac{r}{K} - \frac{\beta((S^* + c) - k_1(I^* + c))}{(S + I + c)(S^* + I^* + c)} \right. \\ & \left. + \frac{P^*(\omega_1 b_1 + \omega_2 k_1)}{(S + b_1 I + c_1)(S^* + b_1 I^* + c_1)} \right) \frac{(S - S^*)^2 + (I - I^*)^2}{2} \\ & = - \left( \frac{3r}{2K} + \frac{\beta((S^* + c) - I^*(k_1 + 2) - k_1 c)}{2(S^* + I^* + c)(S + I + c)} \right. \\ & \left. - \frac{(\omega_1(b_1 + 2) + \omega_2 k_1)P^*}{2(S + b_1 I + c_1)(S^* + b_1 I^* + c_1)} \right) (S - S^*)^2 \\ & - k_1 \left( \frac{r}{2K} + \frac{\beta((3S^* + c) - k_1(I^* + c))}{2(S + I + c)(S^* + I^* + c)} \right. \\ & \left. - \frac{(\omega_2(k_1 + 2b_1) + \omega_1 b_1)P^*}{2(S + b_1 I + c_1)(S^* + b_1 I^* + c_1)} \right) (I - I^*)^2. \end{aligned}$$

Sufficient conditions for  $\frac{dV}{dt}$  to be negative definite require that conditions (3.52) and (3.53) hold. This proves the result.  $\square$

### 3.4. Bifurcation analysis

**Theorem 3.4.** Assume that condition (3.40) holds, then system (2.2) has a Hopf bifurcation near the disease-free equilibrium point  $E_3(\hat{S}, 0, \hat{P})$  as the parameter value  $K$  passes through the critical value  $K_{cr} = \frac{c_1(\delta+\omega_4)}{\omega_4-\delta}$ .

**Proof.** According to the variational matrix  $\mathbf{J}(E_3)$  at the disease-free equilibrium point  $E_3(\hat{S}, 0, \hat{P})$ , the eigenvalues for the equilibrium point  $E_3(\hat{S}, 0, \hat{P})$  can be written as  $\hat{\lambda}_{S,P} = \frac{-B \pm \sqrt{B^2 - 4A}}{2}$  and  $\hat{\lambda}_I = -a - \frac{\omega_2 \hat{P}}{\hat{S} + c_1} + \frac{\beta \hat{S}}{c + \hat{S}}$ , where

$$B = \hat{\lambda}_S + \hat{\lambda}_P = \frac{\delta r(K(\omega_4 - \delta) - c_1(\delta + \omega_4))}{K(\omega_4 - \delta)\omega_4},$$

and

$$A = r\delta \left(1 - \frac{(c_1 + K)\delta}{K\omega_4}\right) > 0.$$

Now it has been shown that  $\lambda_I < 0$  if and only if condition (3.40) holds. However, the eigenvalues  $\lambda_S$  and  $\lambda_P$  are pure imaginary numbers for  $B = 0$  or  $K = K_{cr}$ , so there is a neighborhood around  $K = K_{cr}$  such that  $\lambda_S$  and  $\lambda_P$  can be written as  $\lambda_{S,P} = \theta(K) \pm i\theta_1(K)$ , where  $\theta(K) = \frac{\delta r(K(\omega_4 - \delta) - c_1(\delta + \omega_4))}{K(\omega_4 - \delta)\omega_4}$  represents the real part of  $\lambda_S$  and  $\lambda_P$ . Now since  $[\frac{d\theta(K)}{dK}]_{K=K_{cr}} = \frac{c_1\delta r(\delta + \omega_4)}{K^2(\omega_4 - \delta)\omega_4} \neq 0$ . Therefore, system (2.2) has Hopf bifurcation near the disease-free equilibrium point at  $K = K_{cr}$ . This completes the proof.  $\square$

Now since the predator-free equilibrium point  $E_2$  has two eigenvalues with negative real parts while the third that is given by (3.38) is real and is negative depending on condition (3.39). Then, there is no possibility to have a Hopf bifurcation near this point.

**Theorem 3.5.** When  $\beta = \beta^*$ , then the equilibrium  $E_3$  will be transformed into a non-hyperbolic equilibrium, and the system attains neither a saddle-node bifurcation nor a pitchfork bifurcation, but exhibits a transcritical bifurcation.

**Proof.** One of the eigenvalues of  $\mathbf{J}(E_3)$  will be zero if and only if  $\det \mathbf{J}(E_3) = -a_{13}^{[3]}a_{22}^{[3]}a_{31}^{[3]} = 0$ , i.e.  $a_{13}^{[3]} = 0$ , since  $(a_{13}^{[3]}, a_{31}^{[3]}) \neq (0, 0)$ . This gives  $\beta = \beta^* = \frac{(c+\hat{S})(a(c_1+\hat{S})+P\omega_2)}{\hat{S}(c_1+\hat{S})}$ . The other two eigenvalues are given by  $\hat{\lambda}_{\pm} = \frac{a_{11}^{[3]}}{2} \pm \frac{1}{2}\sqrt{(a_{11}^{[3]})^2 + 4a_{13}^{[3]}a_{31}^{[3]}}$ . We will denote  $\hat{\lambda}_+ = \hat{\lambda}_2$  and  $\hat{\lambda}_- = \hat{\lambda}_3$ . Since  $a_{13}^{[3]} < 0$  and  $a_{31}^{[3]} > 0$ , the real parts of  $\hat{\lambda}_2$  and  $\hat{\lambda}_3$  will be of the same sign as that of  $a_{11}^{[3]}$ . Now, if  $K < K_{cr} = \frac{c_1(\delta+\omega_4)}{(\omega_4-\delta)}$ , then  $a_{11}^{[3]} > 0$  and two eigenvalues of  $\mathbf{J}(E_3)$  will be positive; hence the proof follows from Sotomayor [48].

Again if  $K > K_{cr}$  then  $a_{11}^{[3]} < 0$ . In this case,  $\Omega = (\theta_1, \theta_2, \theta_3)^T$ ,  $\Upsilon = (0, \xi, 0)^T$ , where  $\Omega$  and  $\Upsilon$  are the eigenvectors corresponding to the eigenvalue  $\hat{\lambda}_1 = 0$  of the matrices  $\mathbf{J}(E_3)$  and  $\mathbf{J}(E_3)^T$ , respectively, and  $\theta_1 = -\frac{\hbar_2 a_{32}^{[3]}}{a_{31}^{[3]}}$ ,  $\theta_2 = \hbar_2$ ,  $\theta_3 = \frac{\hbar_2(a_{32}^{[3]}a_{11}^{[3]} - a_{31}^{[3]}a_{12}^{[3]})}{a_{13}^{[3]}a_{31}^{[3]}}$  and  $\hbar_2$ , and  $\xi$  are any two non-zero real numbers [22,48]. Now,  $\Upsilon^T [F_\beta(E_3, \beta^*)] = 0$ , so the system does not experience any saddle-node bifurcations. Again,  $\Upsilon^T [DF_\beta(E_3, \beta^*)\Omega] = \hat{S}_2\hbar_2\theta_2 \neq 0$  and  $\Upsilon^T [D^2F_\beta(E_3, \beta^*)(\Omega, \Omega)] \neq 0$  where  $[DF_\beta(E_3, \beta^*)] = (b_{ij})_{3 \times 3}$ , with  $b_{11} = 0$ ,  $b_{12} = -\hat{S}$ ,  $b_{13} = 0$ ,  $b_{21} = 0$ ,  $b_{22} = \hat{S}$ ,  $b_{23} = 0$ ,  $b_{31} = 0$ ,  $b_{32} = 0$  and  $b_{33} = 0$ .  $D^2F(E_3, \beta^*)$  is a  $3 \times 3 \times 3$  tensor. Thus, by the same theorem the system possesses a transcritical bifurcation [48]. Again,  $\Upsilon^T [D^2F_\beta(E_3, \beta^*)(\Omega, \Omega)] \neq 0$ . Therefore, the system does not experience a pitchfork bifurcation.  $\square$

**Theorem 3.6.** Assume that the conditions (3.41)–(3.44) hold. Then, system (2.2) exhibits a Hopf bifurcation near the positive equilibrium

point  $E^*$  as the parameter  $r$  passes through the critical value  $r_c$  provided that the following condition holds

$$\begin{aligned} S^* &\left( \frac{b_1 P^* \omega_1}{(c_1 + b_1 I^* + S^*)^2} - \frac{r}{K} - (c + S^*)T \right) \\ &\times \left( I^* \left( (c + I^*)T + \frac{P^* \omega_2}{(c_1 + b_1 I^* + S^*)^2} \right) Q \right. \\ &- \left. \frac{I^* P^* \omega_2 (-I^* \omega_3 + (c_1 + b_1 I^*) \omega_4)}{(c_1 + b_1 I^* + S^*)^3} \right) \\ &< \frac{I^* P^* ((c_1 + S^*) \omega_3 - b_1 S^* \omega_4)}{(c_1 + b_1 I^* + S^*)^3} \\ &\times \left( S^* \omega_1 \left( (c + I^*)T + \frac{P^* \omega_2}{(c_1 + b_1 I^* + S^*)^2} \right) + \omega_2 Q \right) \end{aligned} \quad (3.55)$$

where  $T = \frac{\beta}{(S^* + I^* + c)^2}$  and  $Q = -a + S^*(c + S^*)T - \frac{P^*(c_1 + S^*)\omega_2}{(c_1 + b_1 I^* + S^*)^2}$ .

**Proof.** The characteristic equation of  $\mathbf{J}(E^*)$  is given by  $\lambda^3 + A_1\lambda^2 + A_2\lambda + A_3 = 0$ , where  $A_i$ 's;  $i = 1, 2, 3$  are given in Theorem 3.2. It had been observed that conditions (3.41)–(3.44) guarantee that  $A_i > 0$ ;  $i = 1, 2, 3$  for all values of  $r$ .

Since the Hopf bifurcation near the positive equilibrium point  $E^*$  of system (2.2) occurs if and only if  $\mathbf{J}(E^*)$  has two complex conjugate eigenvalues with the third eigenvalue real and negative such that there exists a constant parameter value, say  $r_c$ , the necessary and sufficient conditions for Hopf bifurcation at  $r = r_c$  are  $A_1 > 0$ ,  $A_3 > 0$ ,  $\psi(r_c) = A_1(r_c)A_2(r_c) - A_3(r_c) = 0$  and  $\frac{d\text{Re}(\lambda(r))}{dr}|_{r=r_c} \neq 0$ ; where  $\lambda$  is a complex eigenvalue of  $\mathbf{J}(E^*)$ .

So, by simplifying  $\psi(r_c) = A_1(r_c)A_2(r_c) - A_3(r_c)$  and then equating it to zero we get  $a_{22}^{*2}(a_{11}^{*2})^2 - N_1 a_{11}^{*2} - N_2 = 0$  where  $N_1 = a_{13}^{*2}a_{31}^{*2} + a_{12}^{*2}a_{21}^{*2} - a_{22}^{*2}$  and  $N_2 = a_{12}^{*2}(a_{21}^{*2}a_{22}^{*2} + a_{23}^{*2}a_{31}^{*2}) + a_{32}^{*2}(a_{22}^{*2}a_{23}^{*2} + a_{21}^{*2}a_{13}^{*2})$ , and  $a_{ij}^*$ ;  $i, j = 1, 2, 3$  represents the elements of  $\mathbf{J}(E^*)$ . Obviously  $N_1 < 0$ , while condition (3.55) guarantees that  $N_2 < 0$ . Therefore, by solving the above second order equation we first obtain  $a_{11}^* = \frac{N_1}{2a_{22}^*} + (\frac{1}{2a_{22}^*})\sqrt{N_1^2 + 4a_{22}^*N_2}$ . Substituting the value of  $a_{11}^*$  in this equation and then solving for  $r$  we get that  $r = r_c$ . Accordingly, for  $r = r_c$  we have  $A_1A_2 = A_3$  and then the above characteristic equation can be written as

$$(\lambda^2 + A_2)(\lambda + A_1) = 0. \quad (3.56)$$

For all  $\lambda$ , the roots are generally of the form  $\lambda_1(r) = \eta_1(r) + i\eta_2(r)$ ,  $\lambda_2(r) = \eta_1(r) - i\eta_2(r)$ , and  $\lambda_3(r) = -A_1(r)$ .

Now we shall prove the transversality condition  $\frac{d\text{Re}(\lambda_j(r))}{dr}|_{r=r_c} \neq 0$ ,  $j = 1, 2$ .

Substituting  $\lambda_1(r) = \eta_1(r) + i\eta_2(r)$  into the characteristic equation and calculating the derivative, we have

$$K(r)\eta_1'(r) - L(r)\eta_2'(r) + M(r) = 0, \quad \text{and}$$

$$L(r)\eta_1'(r) + K(r)\eta_2'(r) + N(r) = 0,$$

where

$$K(r) = 3\eta_1^2(r) + 2A_1(r)\eta_1(r) + A_2(r) - 3\eta_2^2(r),$$

$$L(r) = 6\eta_1(r)\eta_2(r) + 2A_1(r)\eta_2(r),$$

$$M(r) = \eta_1^2(r)A_1'(r) + A_2'(r)\eta_1(r) + A_3'(r) - A_1'(r)\eta_2^2(r),$$

$$N(r) = 2\eta_1(r)\eta_2(r)A_1'(r) + A_2'(r)\eta_2(r).$$

Since  $L(r_c)N(r_c) + K(r_c)M(r_c) \neq 0$ , we have  $\frac{d}{dr}(\text{Re } \lambda_j(r))|_{r=r_c} = [\frac{LN+KM}{K^2+L^2}]|_{r=r_c} \neq 0$  and  $\lambda_3 = -A_1 \neq 0$ . Therefore, the transversality condition holds. This implies that a Hopf bifurcation occurs at  $r = r_c$  and is non-degenerate. Biologically, a Hopf bifurcation indicates that the predator population coexists with the susceptible and the infected rabbit populations, exhibiting oscillatory behavior.  $\square$

## 4. Analysis of spatial model system

### 4.1. Linear stability analysis of the SIP spatial model system

For the linear stability analysis of the spatiotemporal model system (2.3), it is perturbed with the following 2-dimensional spatiotemporal perturbations of the form

$$\begin{cases} S = S^* + \epsilon_1 \exp(\lambda_k t + i(k_x x + k_y y)) = S^* + \epsilon_1 s_1, \\ I = I^* + \epsilon_2 \exp(\lambda_k t + i(k_x x + k_y y)) = I^* + \epsilon_2 i_1, \\ P = P^* + \epsilon_3 \exp(\lambda_k t + i(k_x x + k_y y)) = P^* + \epsilon_3 p_1, \end{cases} \quad (4.1)$$

where  $\epsilon_1, \epsilon_2$  and  $\epsilon_3$  are sufficiently small constants,  $k_x$  and  $k_y$  are the components of the wavenumber  $k$  along  $x$  and  $y$  directions respectively, and  $\lambda_k$  is the wavelength.

**Theorem 4.1.** Assume that the parameters in model system (2.3) satisfy conditions (3.41)–(3.45). Then the constant positive steady state  $E^*(S^*, I^*, P^*)$  of the spatiotemporal system is locally asymptotically stable.

**Proof.** The system is linearized about the non-trivial interior equilibrium point  $E^*(S^*, I^*, P^*)$ . The characteristic equation of the linearized version of the spatiotemporal model system (2.3) is given by

$$(J - Dk^2 - \lambda_k I)(s_1, i_1, p_1)^T = 0, \quad (4.2)$$

with

$$J = \begin{bmatrix} a_{11} & a_{12} & a_{13} \\ a_{21} & a_{22} & a_{23} \\ a_{31} & a_{32} & a_{33} \end{bmatrix}, \quad \text{and} \quad D = \begin{bmatrix} D_S & 0 & 0 \\ 0 & D_I & 0 \\ 0 & 0 & D_P \end{bmatrix} \quad (4.3)$$

where  $k$  is the wavenumber given by  $k^2 = k_x^2 + k_y^2$  and  $I$  is a  $3 \times 3$  identity matrix. The entries of the variational matrix  $J$  are the same as those defined in Theorem 3.2. From (4.2) and (4.3), we get the characteristic equation of the form

$$\det(J - Dk^2 - \lambda_k I) = \lambda_k^3 + \rho_1(k^2)\lambda_k^2 + \lambda_k\rho_2(k^2) + \rho_3(k^2) \quad (4.4)$$

where

$$\left\{ \begin{array}{l} \rho_1(k^2) = -\text{tr}(J - Dk^2) = k^2(D_S + D_I + D_P) + A_1, \\ \rho_2(k^2) = k^4(D_S D_I + D_S D_P + D_P D_I) - k^2(D_S(a_{33} + a_{22}) \\ \quad + D_I(a_{11} + a_{33}) + D_P(a_{11} + a_{22})) + A_2, \\ \rho_3(k^2) = -\det(J - Dk^2) = k^6(D_S D_I D_P) \\ \quad + k^4(-D_S D_I a_{33} - a_{22} D_S D_P - a_{11} D_I D_P) \\ \quad + k^2(D_S(a_{33} a_{22} - a_{23} a_{32}) + D_I(a_{11} a_{33} - a_{13} a_{31}) \\ \quad + D_P(a_{11} a_{22} - a_{12} a_{21})) + A_3. \end{array} \right. \quad (4.5)$$

In the above  $A_1$ ,  $A_2$  and  $A_3$  are as defined in (3.47)–(3.49). From assumptions (3.41)–(3.45), it follows that  $\rho_1(k^2) > 0$ ,  $\rho_2(k^2) > 0$  and  $\rho_3(k^2) > 0$ . Algebraic manipulation of the expression  $\rho_1(k^2)\rho_2(k^2) - \rho_3(k^2)$  yields

$$B_1 k^6 + B_2 k^4 + B_3 k^2 + A_1 A_2 - A_3, \quad (4.6)$$

where

$$\left\{ \begin{array}{l} B_1 = (D_S + D_I)(D_S + D_P)(D_I + D_P) > 0, \\ B_2 = -a_{11}(D_I + D_P)(D_I + 2D_S + D_P) \\ \quad - a_{22}(D_S + D_P)(2D_I + D_S + D_P) \\ \quad - a_{33}(D_I + D_S)(D_I + D_S + 2D_P) > 0, \\ B_3 = -(a_{22} + a_{33})A_1 + (a_{11}a_{22} - a_{12}a_{21}) - a_{31}a_{13} + a_{33}a_{11})D_S \\ \quad + (-a_{11} + a_{33})A_1 + (a_{11}a_{22} - a_{12}a_{21}) - a_{23}a_{32} + a_{33}a_{22})D_I \\ \quad + (-a_{22} + a_{11})A_1 + (a_{11} + a_{22})a_{33} - a_{23}a_{32} + a_{13}a_{31})D_P \\ \quad > 0. \end{array} \right.$$

An application of the Routh–Hurwitz criteria gives  $\Re(\lambda(k)) < 0$  if and only if  $\rho_3(k^2) > 0$ ,  $\rho_1(k^2) > 0$  and  $\rho_1(k^2)\rho_2(k^2) - \rho_3(k^2) > 0$ .

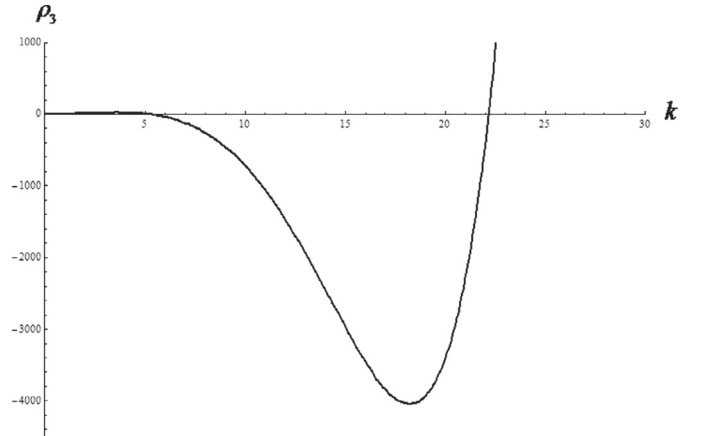


**Fig. 2.** The occurrence of Turing instability as the coefficient ( $\rho_3$ ) of the dispersion relation (4.4) becomes negative for some range of wavenumber  $k$ .

Thus, the constant positive steady state  $E^*(S^*, I^*, P^*)$  of the spatiotemporal system is asymptotically stable.  $\square$

**Remark 4.1.** As a consequence of Theorem 3.2, under conditions (3.41)–(3.45), diffusion cannot destabilize the constant coexistence steady state  $E^*(S^*, I^*, P^*)$  of the system (2.3) and Turing instability cannot occur in the vicinity of  $E^*(S^*, I^*, P^*)$ . Hence system (2.3) will not have a non-constant positive steady state in some neighborhood of  $E^*(S^*, I^*, P^*)$  under conditions (3.41)–(3.45). However, if any one of the conditions (3.41)–(3.45) fails there is a possibility for the occurrence of Turing instability.

**Example 4.1.** For illustrative purposes, let us take the data set  $r = 6.1$ ,  $K = 100$ ,  $\beta = 7.69$ ,  $\omega_1 = 0.5$ ,  $c = 10$ ,  $c_1 = 48$ ,  $\omega_2 = 4.5$ ,  $a = 0.19008$ ,  $\omega_3 = 0.9$ , and  $\omega_4 = 0.12$ ,  $\delta = 0.14$ . It can be shown that for this data set, condition (3.41) fails since  $a_{22} = 0.520863 > 0$  but condition (3.51) ( $A_1 = 1.15116 > 0$ ,  $A_3 = 0.592248 > 0$ ,  $A_1 A_2 - A_3 = 6.80459$ ) still holds and  $E^*(S^*, I^*, P^*)$  is temporally stable. Furthermore,  $\rho_3(k^2)$  changes its sign as the wavenumber  $k$  varies as shown in Fig. 2. In this case, Turing instability is possible. Accordingly, the system may eventually go to a non-constant positive steady state. Thus, the existence of a non-constant positive steady state may be possible when some of the conditions (3.41)–(3.45) fail.

### 4.2. Characterization of the diffusion-driven instability

The spatially homogeneous state will be unstable provided that at least one eigenvalue of the characteristic Eq. (4.4) is positive. It is clear that the homogeneous steady state  $E^*$  is asymptotically stable if and only if  $\rho_1(0) > 0$ ,  $\rho_3(0) > 0$  and  $\rho_1(0)\rho_2(0) - \rho_3(0) > 0$ . But it will be driven to an unstable state by diffusion if any of the conditions

$$\rho_1(k^2) > 0, \quad \rho_3(k^2) > 0 \quad \text{and} \quad \rho_1(k^2)\rho_2(k^2) - \rho_3(k^2) > 0, \quad (4.7)$$

fail to hold. However, it can be easily seen that diffusion-driven instability cannot occur by contradicting  $\rho_1(k^2) > 0$ . Since  $D_S$ ,  $D_I$ ,  $D_P$  and  $k^2$  are all positive, the inequality  $\rho_1(k^2) > 0$  always holds since  $A_1 > 0$  from the stability condition of the interior equilibrium point in homogeneous state. Thus, the system is stable in the absence of diffusion, as a result  $A_1$  is always positive. Hence, we have to look for conditions which reverse the sign of the other two conditions in Eq. (4.7). The expressions for  $\rho_3(k^2)$  and  $\rho_1(k^2)\rho_2(k^2) - \rho_3(k^2)$  are both cubic functions of  $k^2$  of the form  $G(k^2) = G_3 k^6 + G_2 k^4 + G_1 k^2 + G_0$ , such that  $G_3 > 0$ ,  $G_0 > 0$ .

The coefficient  $G_i$  ( $i = 0, 1, 2, 3$ ) for expression of  $\rho_3(k^2) > 0$  and  $\rho_1(k^2)\rho_2(k^2) - \rho_3(k^2) > 0$  are the same as those given in the third

equation of (4.5) and (4.6), respectively. For  $G(k^2)$  to be negative for some positive real number  $k^2 \neq 0$ , the minimum must be negative. This minimum occurs at  $k^2 = k_c^2 = \frac{-G_2 + \sqrt{G_2^2 - 3G_1G_3}}{3G_3}$ . Now  $k_c^2$  is real and positive if

$$G_1 < 0 \quad \text{or} \quad (G_2 < 0 \quad \text{and} \quad G_2^2 > 3G_1G_3). \quad (4.8)$$

Hence

$$G_{\min} = G(K_c^2) = \frac{2G_2^3 - 9G_1G_2G_3 - 2(G_2^2 - 3G_1G_3)^{\frac{3}{2}} + 27G_3^2G_0}{27G_3^2}.$$

Thus

$$G(k_c^2) < 0, \quad \text{if} \quad 2G_2^3 - 9G_1G_2G_3 - 2(G_2^2 - 3G_1G_3)^{\frac{3}{2}} + 27G_3^2G_0 < 0. \quad (4.9)$$

The conditions given in Eqs. (4.8) and (4.9) are sufficient for the occurrence of diffusion-driven instability. The above results are summarized in the following theorem.

**Theorem 4.2.** *The spatial model system (2.3) will undergo diffusion-driven instability at the homogeneous steady state  $E^*$  provided the following conditions are satisfied*

$$G_1 < 0 \quad \text{or} \quad (G_2 < 0 \quad \text{and} \quad G_2^2 > 3G_1G_3),$$

and

$$\left( G_2^3 + \frac{27}{2}G_3^2G_0 - \frac{9}{2}G_1G_2G_3 \right)^2 < (G_2^2 - 3G_1G_3)^3.$$

**Proof.** The proof directly follows from the above derivation.  $\square$

#### 4.3. Global stability of the SIP spatiotemporal model system

To establish the global stability of the positive steady state  $E^*$ , first we recall the following result which can be found in Wang [53].

**Lemma 4.1.** *Let  $a$  and  $b$  be positive constants. Assume that  $\varphi, \psi \in C^1[a, \infty)$ ,  $\psi(t) \geq 0$  and  $\varphi$  is bounded from below. If  $\varphi' \leq -b\psi(t)$  and  $\psi' \leq K \in [a, \infty)$  for some constant  $K$ , then  $\lim_{t \rightarrow \infty} \psi(t) = 0$ .*

Hence, we can state the following result whose proof is given in Appendix A.

**Theorem 4.3.** *The constant positive steady state  $E^*(S^*, I^*, P^*)$  of the spatial model system (2.3) is globally asymptotically stable if the conditions for global stability for the non-spatial model (2.2) hold.*

## 5. Numerical simulations

### 5.1. In the absence of diffusion

In this section, we present detailed numerical simulations of the model system (2.2) in the absence of diffusion. Our aim is to support our theoretical findings resulting from the study of the dynamic behavior of the model system.

The model system (2.2) is integrated using fourth-order Runge-Kutta method under different sets of parameter values and different sets of initial conditions. It is observed that for the following hypothetical set of parameter values  $r = 6.1$ ,  $K = 100$ ,  $\beta = 7.69$ ,  $b_1 = 3$ ,  $\omega_1 = 0.5$ ,  $c = 10$ ,  $c_1 = 48$ ,  $\omega_2 = 4.5$ ,  $a = 0.19008$ ,  $\omega_3 = 0.9$ , and  $\omega_4 = 0.12$ , model system (2.2) possesses different types of attractors as the parameter  $\delta$ , the total death rate of predator population is varied as shown in Fig. 3. The range of values of the parameters are chosen on the basis of the values reported in Jorgensen [30] and in the previous study by Upadhyay et al. [52], Roy and Upadhyay [46], Chattopadhyay et al. [10]. In-spite of the abundant literature on wild rabbit biology, knowledge on basic

biological parameters from natural free populations is still lacking. However, numerical simulations are performed using ecologically permissible parameter values. For example, true conversion rates of  $S$  and  $I$  to  $P$  are set to be  $\omega_4/\omega_1 = 0.24$  and  $\omega_3/\omega_2 = 0.2$ , respectively, which are close to each other. Since, both susceptible and infected rabbits are of the same kind, so these conversion rates must take close values. Alternatively,  $\omega_4/\omega_1 > \omega_3/\omega_2$ , if predation of healthy rabbits leads to more reproduction than that of infected. Also predation coefficients for  $S$  and  $I$  are set to be  $\omega_1 = 0.5$ ,  $\omega_2 = 4.5$ , which indicates that infected rabbits are much frequently attacked by predators than susceptible rabbits. This is based on the fact that rabbits can be caught more easily due to their reduced ability to escape and hence  $\omega_2$  must be larger than  $\omega_1$ . This set of parameter values is kept fixed throughout the numerical experiments.

### 5.1.1. Bifurcation analysis

We have used the Matlab software for plotting the bifurcation diagrams. These bifurcation diagrams are generated by taking the death rate of predator ( $\delta$ ) as bifurcation parameter. Bifurcation diagram of system (2.2) is presented in Fig. 4(a) and (b). In Fig. 4(a), the successive variations of susceptible population ( $S$ ) are taken in the ranges  $0 < S \leq 100$  as a function of  $\delta \in [0, 0.25]$  and the values of other parameters are same as used in Fig. 3. A complex dynamics is observed in the range  $0 \leq \delta \leq 0.048$  and after that the disease dynamics is stable. In Fig. 4(b), the successive variations of infected populations are taken in the ranges  $0 < I \leq 100$  as a function of  $\delta \in [0, 0.25]$ . This diagram also indicates that the model system experiences a transcritical bifurcation at  $\delta = 0.14$  and backward bifurcation (transcritical bifurcation in opposite direction) at some higher value of  $\delta$ . Under the bifurcation analysis, very rich and complex dynamics are observed, presenting various sequences of period-doubling bifurcation leading to chaotic dynamics and sequences of period-halving bifurcation leading to limit cycles.

### 5.2. In the presence of diffusion

#### 5.2.1. 1-D numerical simulations and Turing instability

Next we investigate the effects of adding diffusion to the eco-epidemiological model system (2.2) in 1-dimension. We employ a finite difference numerical method to investigate the effect of diffusion on the model systems. We use the central finite differences in space and a semi-implicit time stepping method [20]. The algorithm is then implemented using the PDEPE routine in MATLAB(R2010). In all the 1-dimensional simulations, we plot space versus population densities to exhibit the spatial dynamics of the model systems.

The equations are numerically solved on a domain of size 7000 with zero flux boundary conditions. We consider initial conditions which determine the initial spatial distributions of the species as  $S(\mathbf{x}, 0) = S^* + \epsilon(\mathbf{x} - \mathbf{x}_1)(\mathbf{x} - \mathbf{x}_2)$ ,  $I(\mathbf{x}, 0) = I^*$ , and  $P(\mathbf{x}, 0) = P^*$ , where  $(S^*, I^*, P^*)$  is the non-trivial state for the co-existence of susceptible and infective rabbit populations.  $\epsilon = 10^{-8}$ ,  $x_1 = 1200$  and  $x_2 = 2800$  are the parameters affecting the system dynamics. The dynamics of the susceptible, infective and predator populations are observed at the fixed parameter values  $r = 6.1$ ,  $K = 100$ ,  $\beta = 7.69$ ,  $\omega_1 = 0.5$ ,  $c = 10$ ,  $c_1 = 48$ ,  $\omega_2 = 4.5$ ,  $a = 0.19008$ ,  $\omega_3 = 0.9$ ,  $\omega_4 = 0.12$  and  $\delta = 0.159928$ . Numerical results are shown at time levels  $t = 200$ ,  $t = 600$  and  $1000$  days, respectively (see Fig. 5). For illustrative purposes, we vary the values of the diffusivity constants  $D_S$  as shown in Fig. 5 (see Table 2 for a complete description of the parameter values).

#### Varying $D_S$ , and $D_P$

Fig. 5 shows that as we increase the value of the diffusivity constant  $D_S$  of the susceptible population, the dynamics of the infected

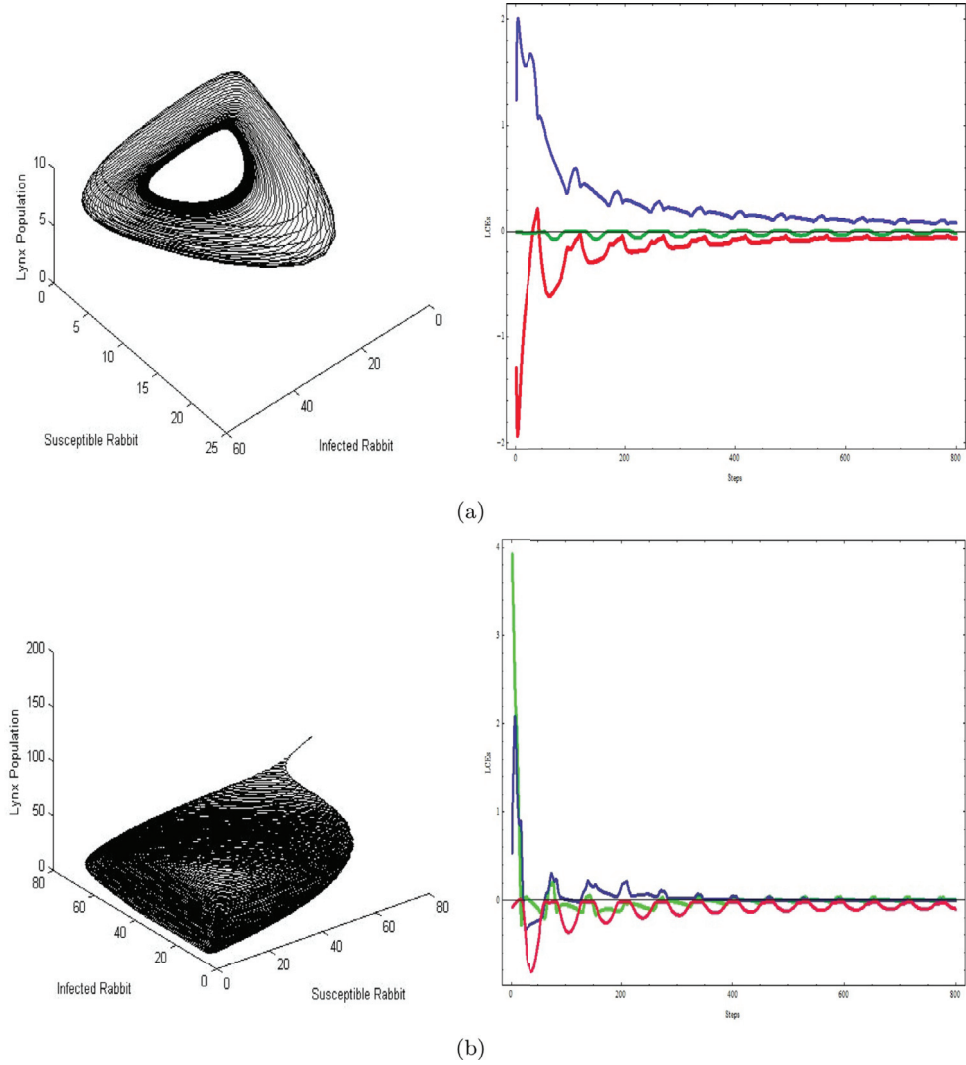


**Fig. 3.** Attractors and convergence plot of the Lyapunov spectrum for different values of the death rate of the predator,  $\delta$  corresponding to model system (2.2) with the rest of the parameter values fixed as outlined in the text. (a) A higher order limit cycle for  $\delta = 0.159928$ , (b) a stable focus attractor for  $\delta = 0.14$ .

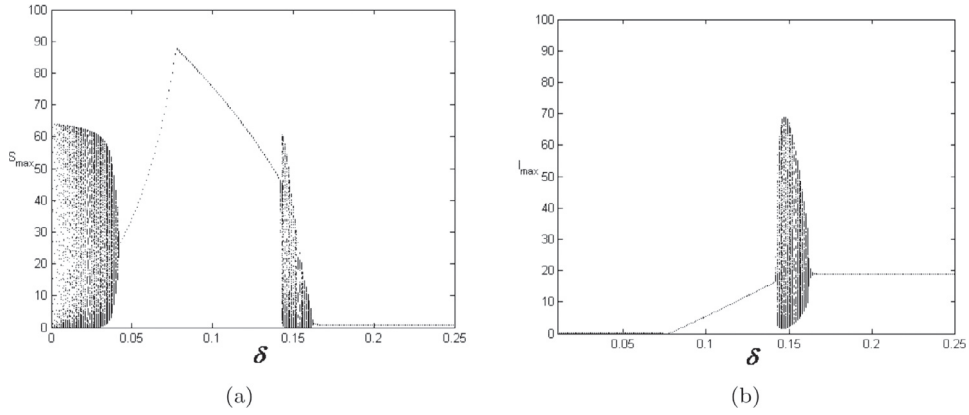


**Fig. 4.** Bifurcation diagrams for a range of values of control parameter  $\delta$  (a)  $S$  (b)  $I$ . The values of other parameters are same as used in Fig. 3.

population becomes chaotic and there is an onset of a chaotic phase for  $D_S = 1$  (see Fig. 5(c)). As we increase the time level from  $t = 200$  (Fig. 5(a) and (b)) to  $t = 600$  days (Fig. 5(c) and (d)), we observe the appearance of a jagged pattern representing chaotic behavior of the system and this grows steadily with time (Fig. 5(c) and (d)). The size of the domain occupied by the irregular chaotic

patterns slowly grows with time in both directions displacing the regular pattern (characterized by a stable limit cycle in the phase plane of the system) with chaotic dynamics (Fig. 5(e) and (f)). This phenomenon has been termed as the “wave of chaos”. The wave of chaos propagates in both forward as well as backward directions. As a result, we predict that the spread of the epidemic will

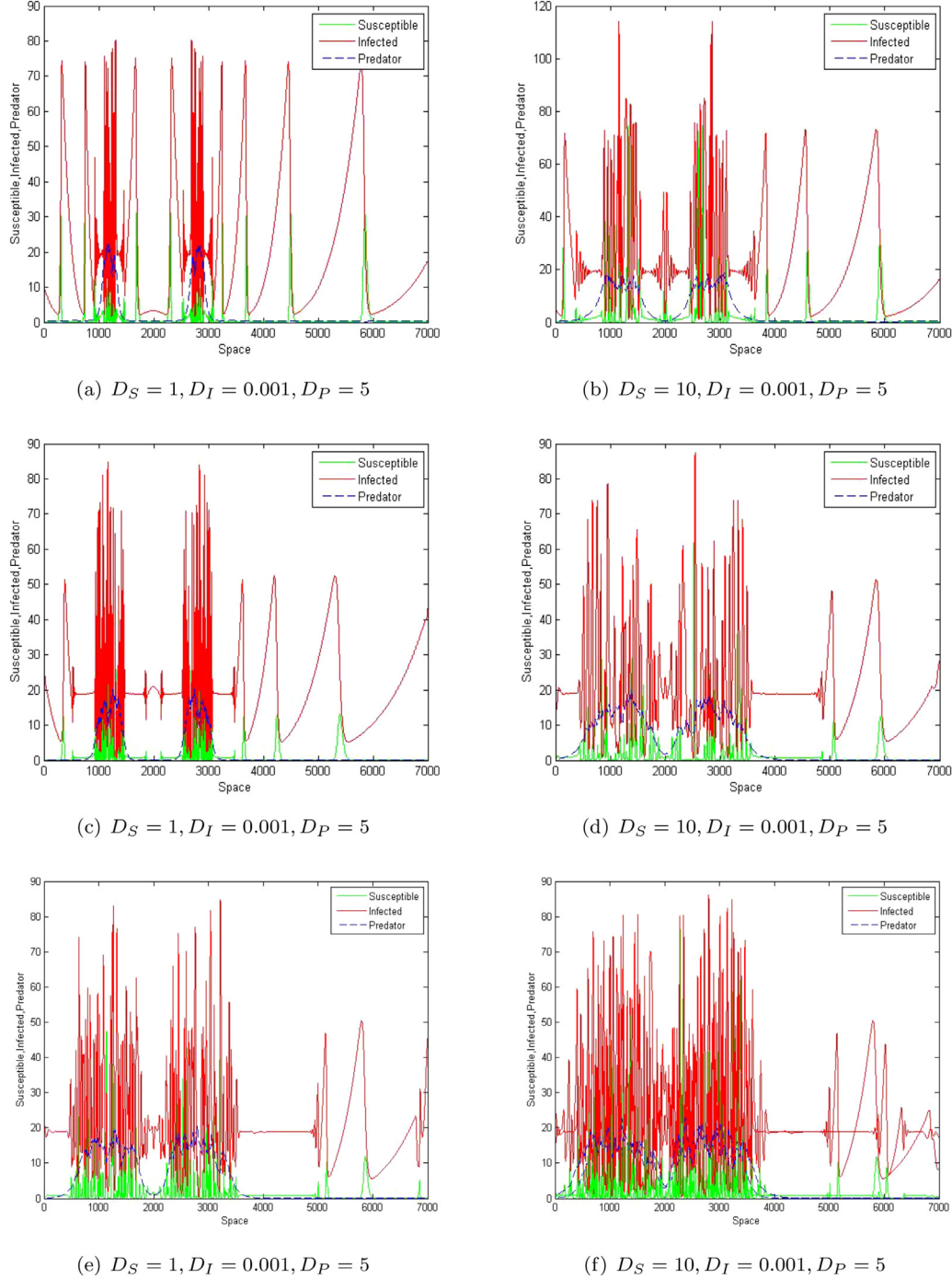


**Fig. 5.** Effect of the diffusivity constant  $D_S$  on rabbit–lynx dynamics of the model system (2.3) exhibiting space series generated at different time (a) and (b)  $t = 200$  days (c) and (d)  $t = 600$  days (e) and (f)  $t = 1000$  days and for different values of  $D_S = 1$  and 10.

be bidirectional. The dynamics of the model system (2.3) lead to the formation of regular spatiotemporal patterns or, through the propagation of the wave of chaos, to the formation of chaotic patterns [41]. This scenario is essentially spatiotemporal: the chaos prevails as a result of the displacement of the regular regime by the chaotic regime. Our numerical results show that the dynamics of the model system at each moment of time have separate regions of chaotic and regular patterns. We observe that chaos arises as a result of the propagation of the wave of chaos, i.e. the moving interface between the two regions. This result shows that a non-stationary irregular pattern appears as the result of the interaction between the three populations. The formation of patterns due

to this scenario corresponds to chaotic dynamics and it leads to the conclusion that spatiotemporal chaos is not a strange or exotic phenomenon but an intrinsic property of disease dynamics. Since chaos means sensitivity to the initial conditions, it means that a long term forecast of the spread of the disease may never be possible.

**Remark 5.1** (varying  $D_P$ ). The numerical simulations show that variations of the diffusivity constant  $D_P$  on the dynamics of the model system results in the emergence of a limit cycle and the onset of chaos (results not shown). The wave of chaos phenomena is observed to emerge as we increase the diffusivity constant  $D_P$ .

**Table 2**

Parameters for the model Eq. (2.2). Default parameter values for the models are chosen midway through the observed range except in cases where the model solutions did not cycle.

Variable	Range	Source	Default value
$r$	1.5–2.0	[27,32,46]	6.1
$K$	50–150	[30,46]	100
$\beta$		[42,46]	7.69
$\omega_1$	0.1–2.0	[27]	0.5
$\omega_4$	0.7–1.0	[32,47]	0.12
$c$		[30,46]	10
$c_1$		[30,45]	48
$b_1$		[30,45]	3
$\omega_2$	0.1–2.0	[27,30,46]	4.5
$\omega_3$	0.7–1.0	[32,47]	0.9
$a$		[30]	0.19008
$\delta$		[30,45]	0.14

**Table 3**

Model parameter values used in the numerical simulations exhibited in Fig. 5.

Figure	$D_S$	$D_I$	$D_P$	The rest of the parameter values are fixed at
5(a), (c) and (e)	1	0.001	5	$r = 6.1, K = 100, \beta = 7.69, \omega_1 = 0.5, c = 10,$ $c_1 = 48, b_1 = 3, \omega_2 = 4.5, a = 0.19008, \omega_3 = 0.9, \omega_4 = 0.12, \delta = 0.159928.$
5(b), (d) and (f)	10	0.001	5	$c_1 = 48, b_1 = 3, \omega_2 = 4.5, a = 0.19008, \omega_3 = 0.9, \omega_4 = 0.12, \delta = 0.159928.$

**Table 4**

Model parameter values used in the numerical simulations shown in Fig. 6.

Figures	$D_S$	$D_I$	$D_P$	$\beta$	Rest of the parameter values
6(a)	1	0.001	5	6.5	$r = 6.1, K = 100, b_1 = 3, \omega_1 = 0.5,$
6(b)	1	0.001	5	6.79	$c = 10, c_1 = 48, \omega_2 = 4.5, a = 0.19008,$
6(c)	1	0.001	5	7	$\omega_3 = 0.9, \omega_4 = 0.12, \delta = 0.159928.$

**Table 5**

Model parameter values used in numerical simulations illustrated in Fig. 7.

Figs. no.	$D_S$	$D_I$	$D_P$	Rest of the parameter values
7(a)	0.5	0.005	5	$r = 6.1, K = 100, \beta = 7.69, b_1 = 3,$
7(b)	1	0.005	5	$\omega_1 = 0.5, c = 10, c_1 = 48, \omega_2 = 4.5,$
7(c)	15	0.005	5	$a = 0.19008, \omega_3 = 0.9, \omega_4 = 0.12, \delta = 0.14.$

### Effect of the transmission rate $\beta$

The dynamics of the model system for the 1-dimensional case are observed at the same time level  $t = 200$  and for the set of parameter values shown in Table 3. We take different values of  $\beta = 6.5, 6.79, 7$  with corresponding  $R_0 = 0.843692, 0.847485$  and  $0.850937$ , respectively. In Fig. 6, we observe that as  $\beta$  increases the system changes its behavior from stable, periodic to chaotic. We also observe that the disease persists in space and its spread increases with an increase in  $R_0$ .

These figures show that increasing  $D_S$  from 1 to 10, the regular distribution of lynx population at a fixed time starts showing irregular behavior in the space. Similar kind of behavior is observed when  $\beta$  is increased. Our simulation suggests that the movement of rabbit population is beneficial for the survival of lynx population while  $\beta$  should be kept low in order to maintain the uniform distribution of the lynx species in the entire domain.

### 5.2.2. Turing instability

Next, we compute Turing patterns corresponding to model system (2.3) for appropriate model parameter values as detailed given in Tables 5 and 6, respectively. In all our computations, initial conditions are prescribed as small random perturbations around the positive uniform steady state  $E^*$ . Although Turing instability may

**Table 6**

Model parameter values used in numerical simulations exhibited in Fig. 8.

Figures	$\beta$	Rest of the parameter values
8(a)	6.79	$r = 6.1, K = 100, \beta = 7.69,$
8(b)	7	$\omega_1 = 0.5, c = 10, c_1 = 48, \omega_2 = 4.5,$
8(c)	7.69	$a = 0.19008, \omega_3 = 0.9, \omega_4 = 0.12, \delta = 0.14.$

exist for other uniform steady states, here we focus solely on  $E^*$ . Zero-flux (also known as homogeneous Neumann) boundary conditions are imposed. In Table 5, we present the different values of the diffusion coefficients selected to generate different Turing patterns. Numerical simulations exhibiting Turing patterns are shown and presented as contour plots in Fig. 7. We observe that all the three populations are distributed as spatial patterns for lower values of the diffusion coefficient  $D_S = 0.5$ . As we increase  $D_S$  to a moderate ( $D_S = 1$ , see Fig. 7(b)) and high values ( $D_S = 15$ , see Fig. 7(c)), the initial pattern evolves to no pattern (convergence to the uniform state) for lynx populations while the rabbit population (susceptible, infected) show alternate high and low density distribution. From simulation we can observe that the lynx population is distributed in the whole spatial domain with maximum population density below the time level  $t = 50$ . Similar patterns are obtained when the diffusion coefficients  $D_I$  and  $D_P$  are varied (results not shown).

Fig. 8, shows the effect of the contact rate  $\beta$  on the spatio-temporal distribution of all the three populations. We find that as we increase  $\beta$ , the susceptible rabbit population density and the infected rabbit density shows alternate low and high density distribution while the lynx population distribution remains the same. From these figures, we also observe that as  $\beta$  increases the lynx population density remains uniform throughout the domain. These figures also show that maximum density of susceptible rabbits attracts more predator at initial time. We also observe that as  $\beta$  increases Iberian lynx population also increases. This may be due to the fact that infected rabbit are weak and easily available. But if  $\beta$  is increased beyond a critical value the lynx population will decline due to scarcity of food. These figures give hope that transmission incorporating spatial and social limitation can save Iberian lynx from extinction. Therefore, for conserving the lynx population it has been suggested to control the transmission of RHDV by disinfection, depopulation, surveillance and quarantines to effectively eradicate the infected rabbit population.

We numerically validate that each of the patterns presented are indeed Turing patterns. This is done by checking the planar stability; that is, for the wave-number  $k = 0$ ,  $A_n(k = 0) > 0$  for all  $n$ , and  $A_1(0)A_2(0) > A_3(0)$ : however there exists at least one mode, such that for some  $k > 0$ , one or more of the conditions  $A_1(k) > 0, A_3(k) > 0, A_1(k)A_2(k) > A_3(k)$  is or are violated.

The model without diffusion, exhibits stable dynamics for certain parameter values but these can be destabilized to chaos through the inclusion of diffusion. We numerically test this observation in Fig. 9. Here parameter values are chosen as  $r = 6.1, K = 100, \beta = 7.69, \omega_1 = 0.5, c = 10, c_1 = 48, \omega_2 = 4.5, a = 0.19008, \omega_3 = 0.9, \omega_4 = 0.12$  and  $\delta = 0.1$ . We observe the formation of a stable focus as shown in Fig. 9(a). Imposing diffusion in the three species model with  $D_S = 0.5, D_I = 0.001$  and  $D_P = 5$  shows that the stable dynamics become chaotic as shown in Fig. 9(b).

### 5.3. 2-D numerical simulations and Turing patterns of the model system

We now present Turing patterns for the model system (2.3) in two dimensions. These patterns are computed using a finite element numerical method for the spatial discretization with

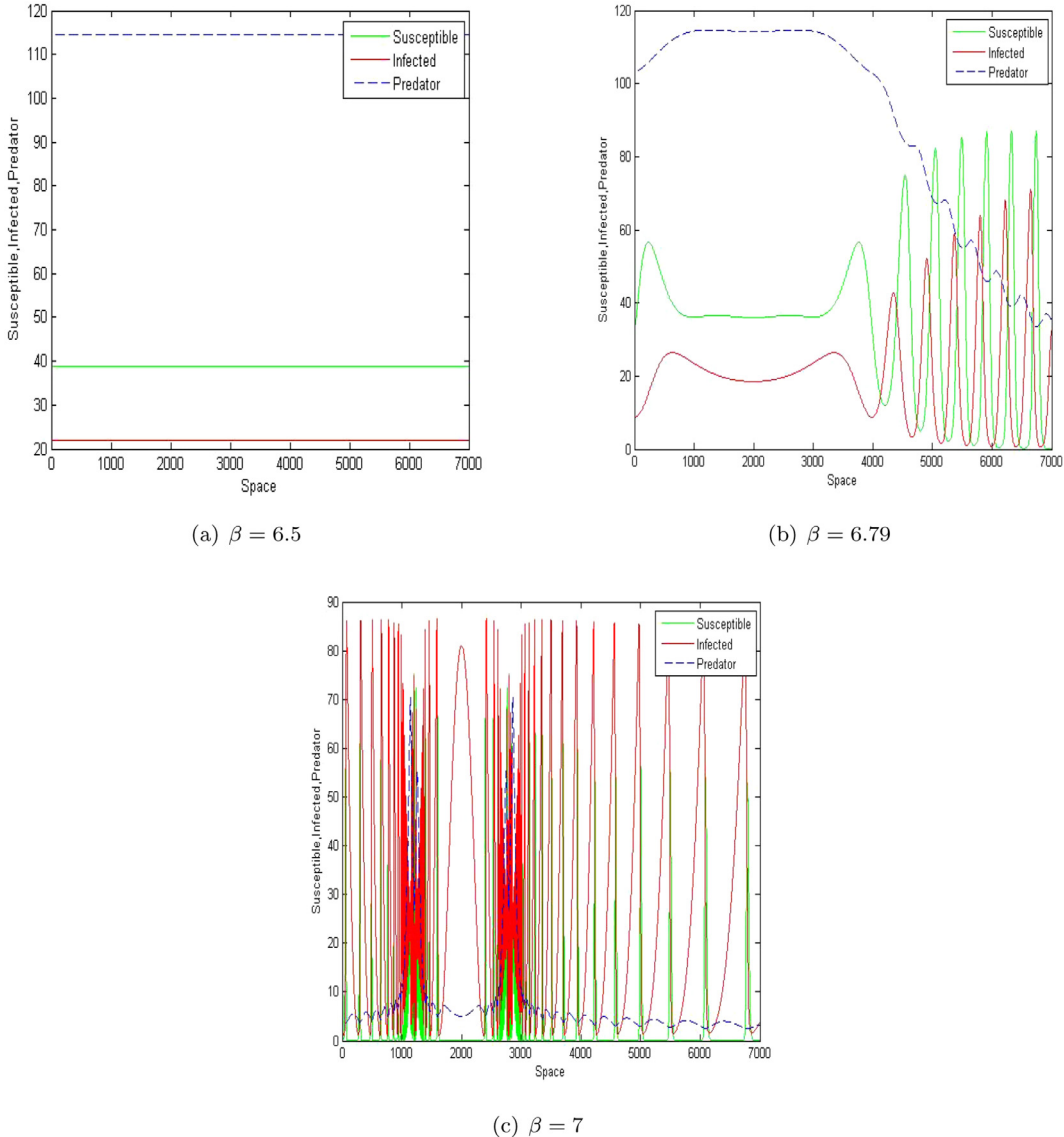


**Fig. 6.** Numerical solutions corresponding to the model system (2.3) exhibiting space series generated at time (a)–(c)  $t = 200$ , showing the effect of varying  $\beta$  on the rabbit-lynx dynamics. The rest of the parameter values are shown in Table 4.

implicit-explicit time-stepping as described and analyzed in [33]. As in the previous sections, the initial conditions for all of our calculations are based on small random perturbations of the positive uniform steady state  $E^*$  and homogeneous Neumann (zero-flux) boundary conditions are imposed. All of the simulations are carried out on a triangulation of the  $10 \times 10$  square using a mesh with 33,025 degrees of freedom and a time-step of  $10^{-2}$ . Fig. 10 shows the patterns generated as we vary the susceptible diffusion coefficient with the remaining parameter values given in the figure captions. We observe, as usual with Turing patterns, transitions from stripe to spot patterns as the diffusion coefficient is varied. Rigorous mathematical analysis of the transition of patterns from say spots to stripes or vice versa is beyond the scope of this study. Interestingly, increasing the susceptible diffusivity as shown in Fig. 10 appears to yield patterns with lower wave-numbers. In Fig. 11 we report on the results of simulations where we vary the parameter  $\beta$ . We clearly observe an increase in the wavenumber of the resultant patterns as we increase the parameter  $\beta$  from 1.69 to 7.69. This increase in wavenumber represents the large groups of all the population are divided into small groups on increment of  $\beta$ . From these figure we observe that Iberian lynx are mainly

present in the domain where the density of infected rabbit population is more. Biologically, this makes sense as infected rabbit are weak and can be captured easily so it will attract a large number of Iberian lynx in that region. Here also we observe that as  $\beta$  increases the density of the predator population increases and gets concentrated on the boundary of the domain but with further increment of  $\beta$  the susceptible rabbit and lynx population gets extinct with uniform distribution of infected rabbit over the whole domain (result now shown here). Therefore, controlling the transmission of RHDV beyond a threshold limit is recommended.

It worth remarking that the numerical results presented in this work are independent of the choice of the numerical method. We have obtained similar results when the finite differences (for both 1-D and 2-D case) is employed. Refining the time- or space-discretizations yield similar results.

## 6. Discussions and conclusions

The Iberian lynx provides an opportunity to learn about extinction dynamics in a changing world, where nature conservation is an increasing public demand. The Iberian lynx can act as

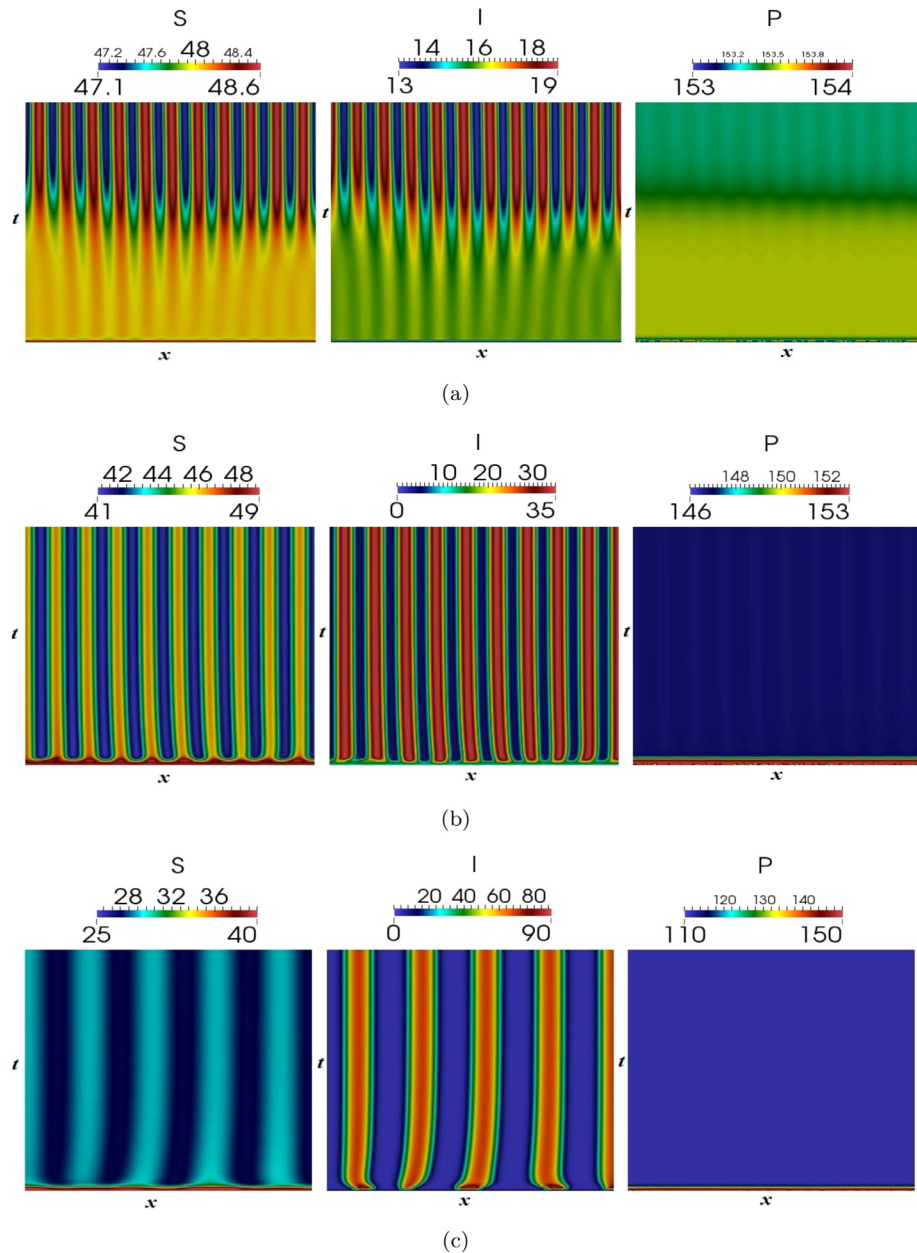


**Fig. 7.** Finite element numerical results of the model system (2.3) showing the densities of the three species as contour plots in the  $x$ - $t$  plane with (a):  $D_S = 0.5$ ,  $D_I = 0.005$ ,  $D_P = 5$ , (b):  $D_S = 1$ ,  $D_I = 0.005$ ,  $D_P = 5$  and (c):  $D_S = 15$ ,  $D_I = 0.005$ ,  $D_P = 5$ .

model for the conservation of other, little-known felid species. In this paper, we have proposed and analyzed a three species eco-epidemiological model for susceptible rabbit, infected rabbit and predator (Iberian lynx) populations. The non trivial equilibrium  $E^*$  of the predator-prey coexistence is locally as well as globally asymptotically stable under a fixed region of attraction when certain conditions are satisfied. The equilibrium states are characterized and the existence of a Hopf-bifurcation is established. Our theoretical and computational results show that the model exhibits rich dynamics. We have also studied the reaction-diffusion model in both one- and two-dimensions and investigated its stability as well as establishing conditions for diffusion-driven instability. The disease-free equilibrium state  $E_3$  is locally as well as globally asymptotically stable in a fixed region of attraction when certain conditions are satisfied. It is found that the infection-free steady state  $E_3$  is epidemiologically unstable if  $R_0$ , the basic reproduction number is greater than one. The necessary condition for the local

stability of  $E_3$  is that  $R_0 < 1$ , which implies that the infected rabbit will become extinct and consequently the disease will be eradicated from the rabbit-lynx system. When transmission rate  $\beta$ , attains a critical value, the equilibrium  $E_3$  is transformed into a non-hyperbolic equilibrium, and the system exhibits a transcritical bifurcation. Some studies have reported that parasite could change the external feature or behavior of the prey, causing extended vulnerability to predation [23,28]. Here we study the changes in dynamics of a predator population, which lives on a native rabbit prey that carries some infection. Since lynx feeds both susceptible and infected rabbits, the multiple prey type II response function was used. Our aim was to study the changes in dynamical properties of predator and rabbit prey species under these realistic assumptions.

Despite national and international efforts, the lynx numbers have fallen by at least 80%, from 1000 to less than 200, between 1980 and 2008. The Iberian lynx and European rabbit are his-

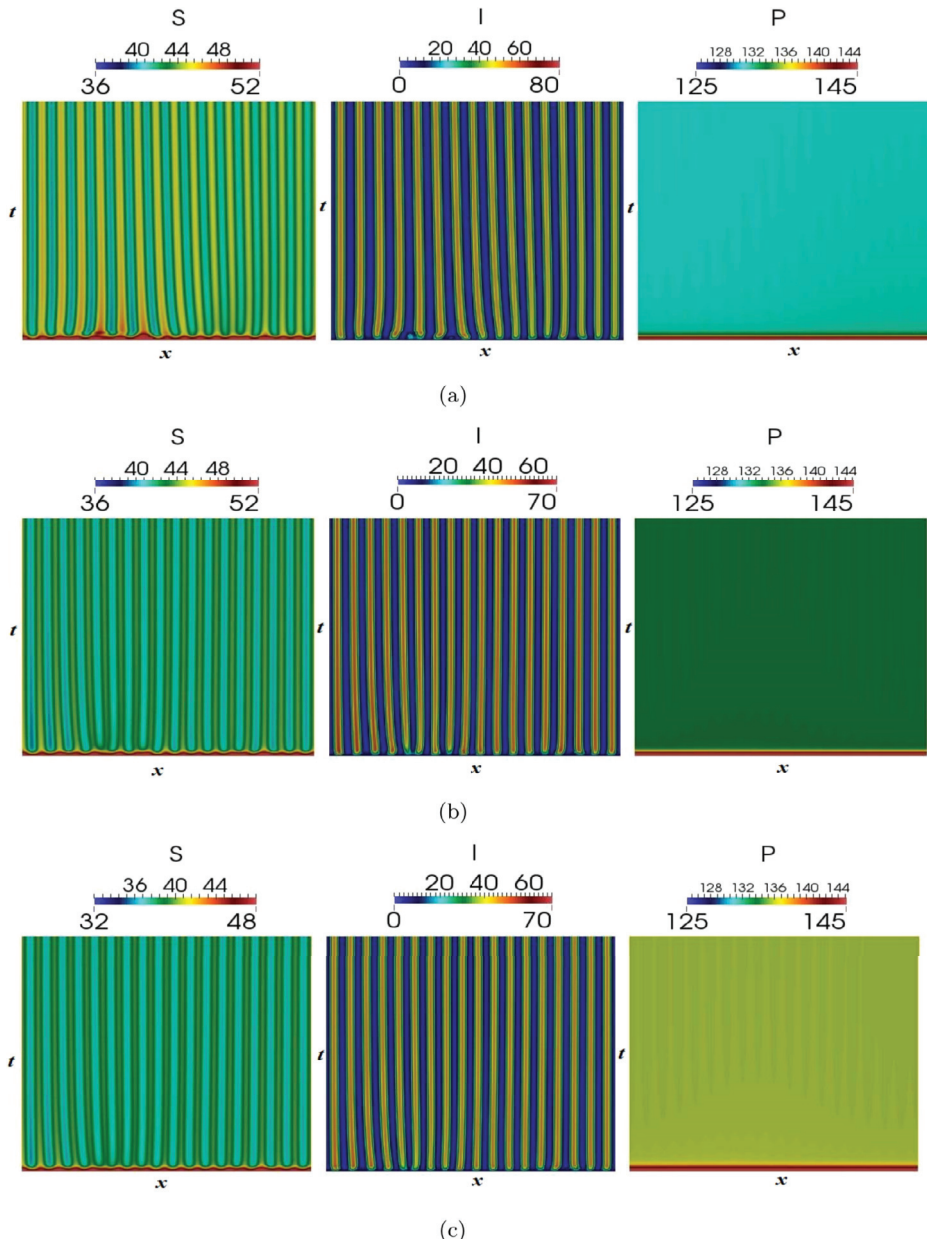


**Fig. 8.** Finite element numerical results of the model system (2.3) showing the densities of the three species as contour plots in the  $x$ - $t$  plane with (a):  $\beta = 6.79$ , (b):  $\beta = 7$  and (c):  $\beta = 7.69$ .

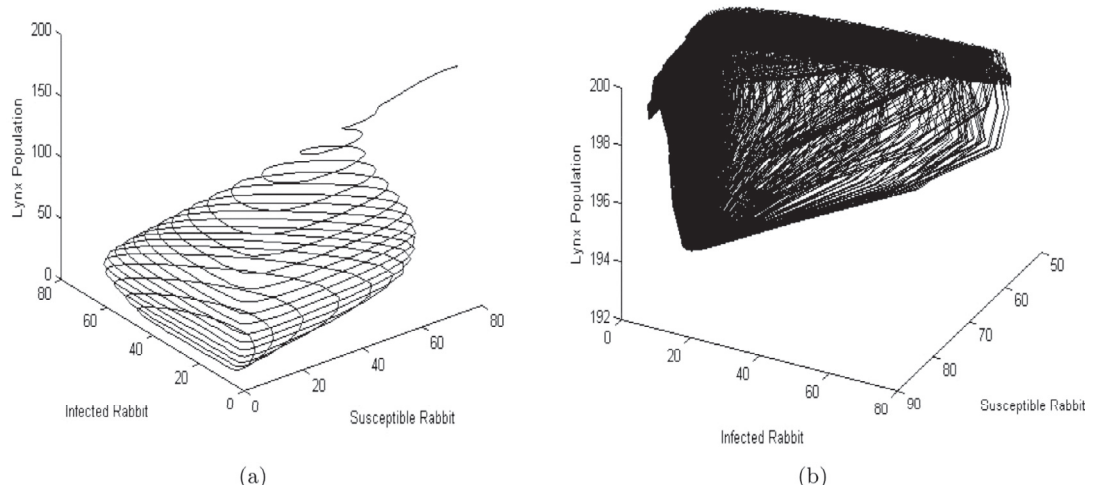


**Fig. 9.** (a) Stable focus of the system in the absence of diffusion. (b) Strange attractor of the system in the presence of diffusion.

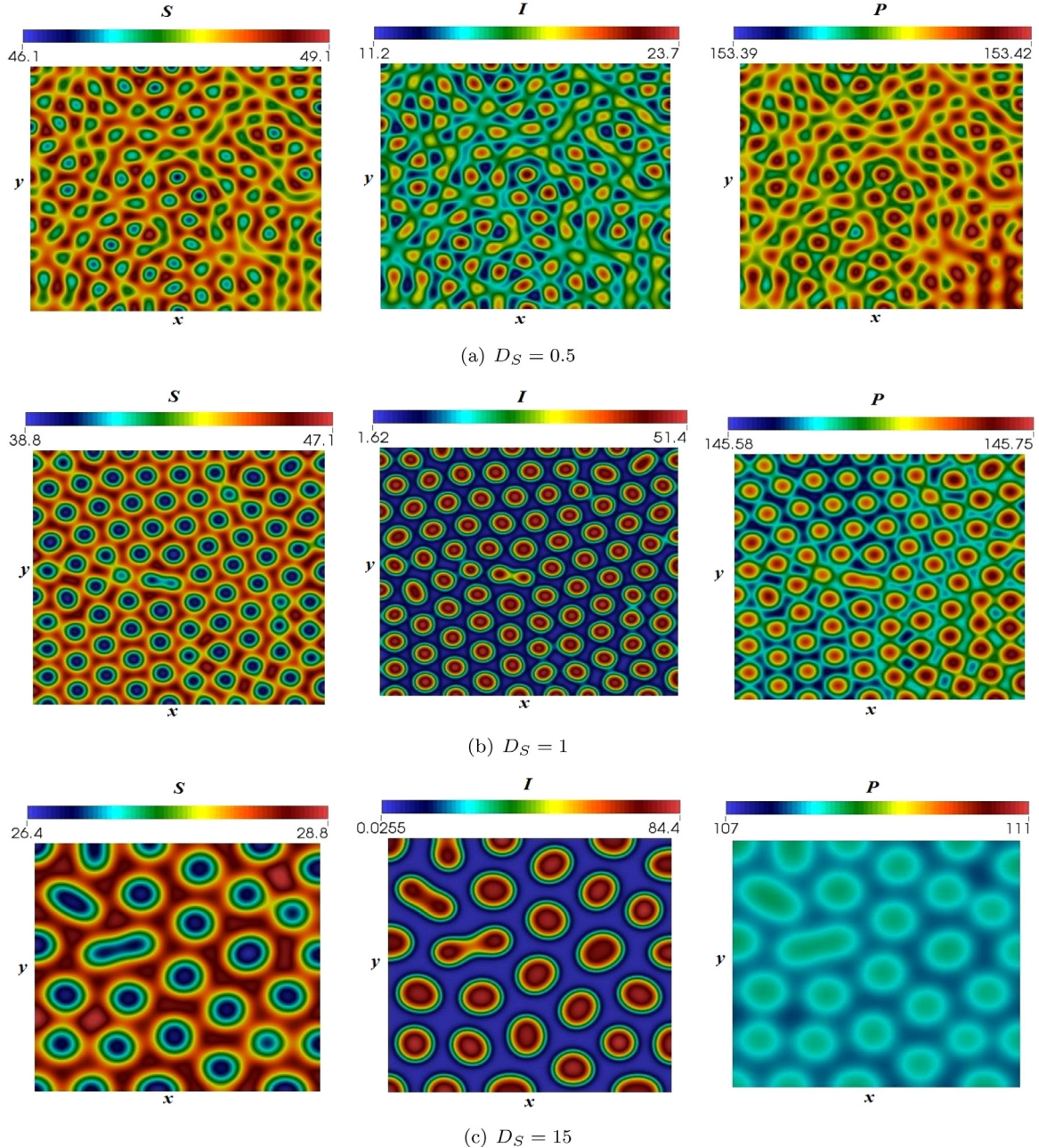


**Fig. 10.** 2-D numerical results of the model system (2.3) showing the snapshots of the densities of the three species at  $t = 1000$  days. The values of the susceptible rabbit diffusion coefficient  $D_S$  are given in the subfigure captions. The remaining parameter values are fixed in each simulation as  $D_I = 0.005$ ,  $D_P = 5$ ,  $r = 6.1$ ,  $K = 100$ ,  $\beta = 7.69$ ,  $\omega_1 = 0.5$ ,  $c = 10$ ,  $c_1 = 48$ ,  $b_1 = 3$ ,  $\omega_2 = 4.5$ ,  $a = 0.19008$ ,  $\omega_3 = 0.9$ ,  $\omega_4 = 0.12$  and  $\delta = 0.14$ .

torically related species, and share the same geographical origin. Eco-epidemiological modeling using reaction-diffusion models can help us to understand the distribution of rabbit and Iberian lynx population in both space and time. We investigated the spatiotemporal dynamics of the reaction-diffusion model by varying the contact rate  $\beta$ , as well as varying the diffusion coefficients  $D_S$ ,  $D_I$  and  $D_P$ , corresponding to the susceptible, infected and predation populations, respectively. In all the simulations exhibiting diffusion-driven instability we observe that the susceptible densities are out of phase with the infected and predator densities. By varying the diffusivities of the different species we observe a variety of different Turing patterns in 1D and 2D. For example in the 2D simulations we observe striking transitions from stripes to spots as the diffusivity of the susceptibles is increased. Similarly

spots give way to labyrinthine patterns which revert back to spots as the predator diffusivity is increased (results not shown). Interestingly the results in Fig. 10 suggest that increasing the diffusivity of the susceptibles and the infected has opposite effects, with an increase in  $D_S$  generating patterns with a higher wavenumber while an increase in  $D_I$  generates patterns with a lower wavenumber. This may be expected as the linear stability analysis of Section 4 illustrates the inhibitory role played by the susceptible while the infected show a combination of activator and inhibitory effects. Thus, increasing  $D_S$  may be regarded as increasing the range of the inhibition and hence driving the system further towards the *short-range activation long-range inhibition* state that is characteristic of Turing patterns. As we increase the contact rate  $\beta$  (whilst remaining in the diffusion-driven instability regime) we ob-

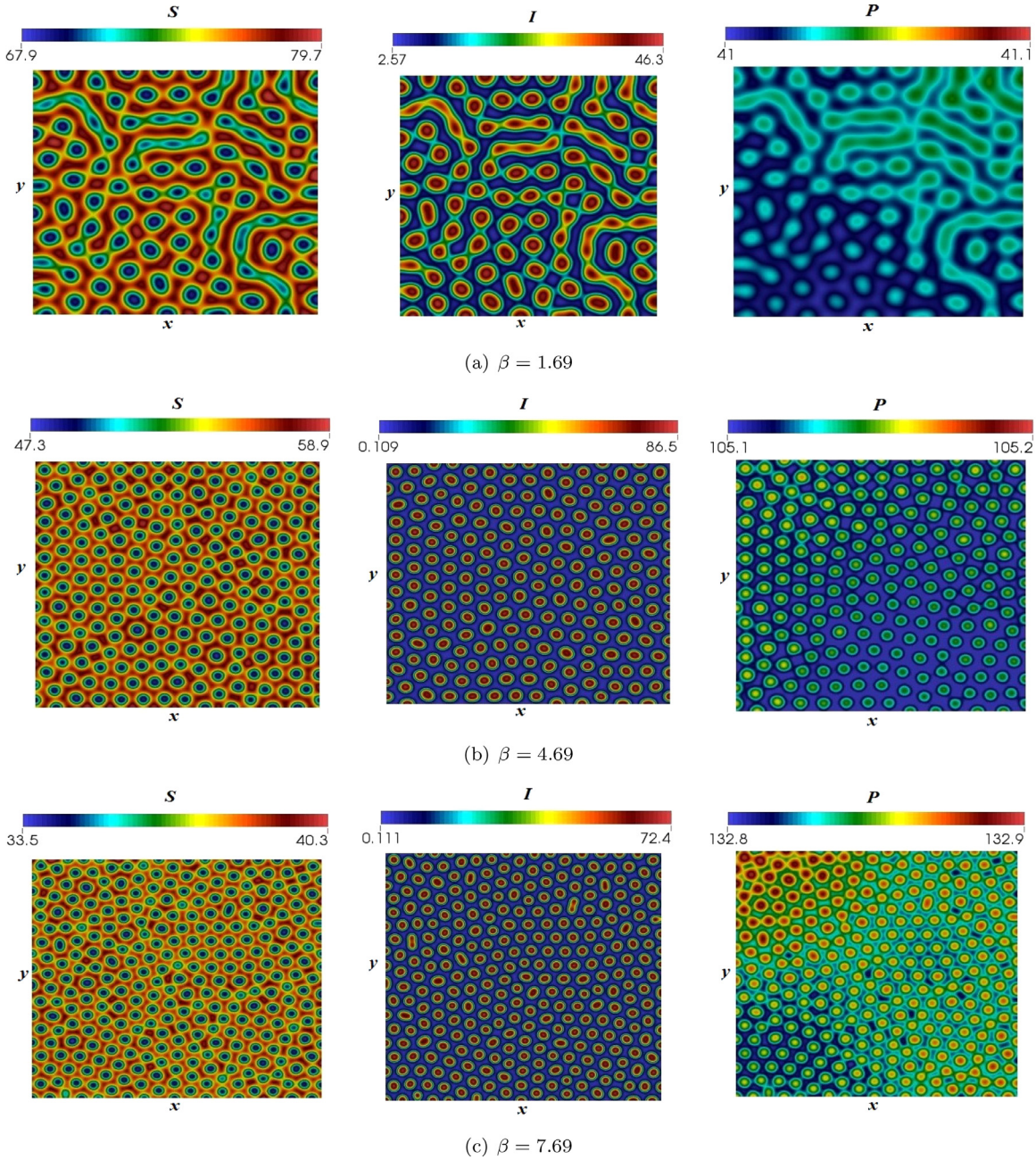


**Fig. 11.** 2-D numerical results of the model system (2.3) showing the snapshots of the densities of the three species at  $t = 1000$  days. The values of the parameter  $\beta$  are given in the subfigure captions. The remaining parameter values are fixed in each simulation as  $D_S = 5$ ,  $D_I = 0.005$ ,  $D_P = 10$ ,  $r = 6.1$ ,  $K = 100$ ,  $\beta = 7.69$ ,  $\omega_1 = 0.5$ ,  $c = 10$ ,  $c_1 = 48$ ,  $b_1 = 3$ ,  $\omega_2 = 4.5$ ,  $a = 0.19008$ ,  $\omega_3 = 0.9$ ,  $\omega_4 = 0.12$  and  $\delta = 0.14$ .

serve patterns of increasing complexity with higher wavenumbers (see Fig. 11 for details) suggesting that the contact rate plays a significant role in the spatial distribution of the species even in a Turing pattern formation setting. Our numerical simulation suggests that one solution to this conservation problem could be restoring the distributions of the two species. Our results suggest that some areas where infected rabbit population are mostly present could be considered lynx reintroduction, even if they are not the most recently inhabited by lynxes. Human and spatial variables also play a significant role in restricting the lynx number rather than the rabbit scarcity. Our main focus should be in learning how to restore the ecological conditions that allow lynx settlement and reproduction. Our simulation also suggests that modified transmis-

sion rate which incorporates limitation in infection due social and spatial distribution helps to maintain the population balance.

Furthermore, our analytical results show that chaotic dynamics remain chaotic under the action of diffusion. However, stable dynamics may become chaotic in the diffusive case. Thus, diffusion in all the three population is seen to have a destabilizing influence, depending on the parameter values and the diffusion coefficients. This in accordance with the results obtained by Pascual [40]. Our analytical and numerical simulations suggest that the disease transmission coefficient  $\beta$  plays an important role in the persistence of the population. Here our focus was on system parameters to get control over extinction of lynx population due to RHD rather than the control from outside, like vaccination. It is very difficult to implement massive rabbit vaccination program in-

volving risk and delay. It is, therefore, important to take necessary preventive measures using the in-built system controls like disease contact rate, predators death rate etc. with the prior knowledge of the disease dynamics. Therefore, efforts need to be made to increase knowledge in some research fields, which are fundamental to correctly manage these species in the wild. Conservationists need to assess the costs versus the benefits of vaccinating wild rabbits against viral diseases and assess whether it would actually improve the status of the local rabbit population. In the long-term more efforts should be made to monitor the immunological status of the population or body condition, as sanitary indicators of the population. Finally, probably one of the most urgent management measures to implement is a working platform gathering researchers, hunters and conservationists for the definition of a global strategy that defends collective interests and serves the goal of conserving this lagomorph without which future lynx reintroductions will be compromised. We hope that our results will enhance the understanding of spatial epidemiology and conservation problem.

## Acknowledgments

This work is supported by University Grants Commission, Govt. of India under Grant no. F. No. 42-16/2013(SR) to the first author (R.K. Upadhyay). AM and CV would like to acknowledge support from the Engineering and Physical Sciences Research Council Grant (EP/J016780/1) and the Leverhulme Trust Research Project Grant (RPG-2014-149). AM is also grateful for support from the EU Horizon2020 MSCA-ITN-2014 Grant, InCeM (Proposal no. 642866).

## Appendix A. Proof of Theorem 4.3

In the following,  $C$  denotes the positive constant which does not depend on  $x \in \bar{\Omega}$  and  $t \geq 0$ . As the solution  $u(\cdot, t)$  of (2.3) is bounded uniformly on  $\bar{\Omega}$ , that is,  $\|u(\cdot, t)\|_{\infty} \leq C$  for all  $t \geq 0$  then according to Lv et al. [34], Wang [53] we have

$$\|u_i(\cdot, t)\|_{C^{2,\alpha}}(\bar{\Omega}) \leq C, \quad \text{for all } t \geq 0. \quad (6.1)$$

Let us define a positive definite Lyapunov function

$$\begin{aligned} V(t) = & \int_{\Omega} \left( S - S^* - S^* \ln \frac{S}{S^*} \right) + k_1 \left( I - I^* - I^* \ln \frac{I}{I^*} \right) \\ & + k_2 \left( P - P^* - P^* \ln \frac{P}{P^*} \right) dx. \end{aligned}$$

Then  $V(t) \geq 0$  for all  $t \geq 0$ . Using model system (2.3) and integrating by parts, we have

$$\begin{aligned} V'(t) = & - \int_{\Omega} \left\{ \frac{D_S S^*}{S^2} |\nabla S|^2 + k_1 \frac{D_I I^*}{I^2} |\nabla I|^2 + k_2 \frac{D_P P^*}{P^2} |\nabla P|^2 \right\} dx \\ & + \int_{\Omega} \left\{ \frac{S - S^*}{S} \frac{dS}{dt} + k_1 \frac{I - I^*}{I} \frac{dI}{dt} + k_2 \frac{P - P^*}{P} \frac{dP}{dt} \right\} dx. \quad (6.2) \end{aligned}$$

From the stability analysis of model system (2.2) we note that

$$\begin{aligned} & \frac{S - S^*}{S} \frac{dS}{dt} + k_1 \frac{I - I^*}{I} \frac{dI}{dt} + k_2 \frac{P - P^*}{P} \frac{dP}{dt} \\ & \leq - \left( \frac{3r}{2K} + \frac{\beta((S^* + c) - I^*(k_1 + 2) - k_1 c)}{2(S^* + I^* + c)(S + I + c)} \right. \\ & \quad \left. - \frac{(\omega_1(b_1 + 2) + \omega_2 k_1)P^*}{2(S + b_1 I + c_1)(S^* + b_1 I^* + c_1)} \right) (S - S^*)^2 \\ & \quad - k_1 \left( \frac{r}{2K} + \frac{\beta(3S^* + c) - k_1(I^* + c)}{2(S + I + c)(S^* + I^* + c)} \right. \\ & \quad \left. - \frac{(\omega_2(k_1 + 2b_1) + \omega_1 b_1)P^*}{2(S + I + c)(S^* + I^* + c)} \right) (I - I^*)^2 dx. \end{aligned}$$

$$- \frac{(\omega_2(k_1 + 2b_1) + \omega_1 b_1)P^*}{2(S + I + c)(S^* + I^* + c)} \Big) (I - I^*)^2.$$

Therefore

$$\begin{aligned} V'(t) \leq & - \int_{\Omega} \left\{ \frac{D_S S^*}{S^2} |\nabla S|^2 + k_1 \frac{D_I I^*}{I^2} |\nabla I|^2 + k_2 \frac{D_P P^*}{P^2} |\nabla P|^2 \right\} dx \\ & + \int_{\Omega} - \left( \frac{3r}{2K} + \frac{\beta((S^* + c) - I^*(k_1 + 2) - k_1 c)}{2(S^* + I^* + c)(S + I + c)} \right. \\ & \quad \left. - \frac{(\omega_1(b_1 + 2) + \omega_2 k_1)P^*}{2(S + b_1 I + c_1)(S^* + b_1 I^* + c_1)} \right) (S - S^*)^2 dx \\ & - k_1 \left( \frac{r}{2K} + \frac{\beta(3S^* + c) - k_1(I^* + c)}{2(S + I + c)(S^* + I^* + c)} \right. \\ & \quad \left. - \frac{(\omega_2(k_1 + 2b_1) + \omega_1 b_1)P^*}{2(S + I + c)(S^* + I^* + c)} \right) (I - I^*)^2 dx. \end{aligned}$$

Since  $u_i^2 \leq C$ , it follows that

$$V'(t) \leq T_1 + T_2 + T_3 = -\psi_1(t) - \psi_2(t), \quad (6.3)$$

where

$$\begin{aligned} T_1 = & - \frac{1}{C} \int_{\Omega} \{ |\nabla S|^2 + |\nabla I|^2 + |\nabla P|^2 \} dx, \\ T_2 = & - \int_{\Omega} \left( \frac{3r}{2K} + \frac{\beta((S^* + c) - I^*(k_1 + 2) - k_1 c)}{2(S^* + I^* + c)(S + I + c)} \right. \\ & \quad \left. - \frac{(\omega_1(b_1 + 2) + \omega_2 k_1)P^*}{2(S + b_1 I + c_1)(S^* + b_1 I^* + c_1)} \right) (S - S^*)^2 dx \\ T_3 = & - \int_{\Omega} k_1 \left( \frac{r}{2K} + \frac{\beta(3S^* + c) - k_1(I^* + c)}{2(S + I + c)(S^* + I^* + c)} \right. \\ & \quad \left. - \frac{(\omega_2(k_1 + 2b_1) + \omega_1 b_1)P^*}{2(S + I + c)(S^* + I^* + c)} \right) (I - I^*)^2 dx. \end{aligned} \quad (6.4)$$

From Eqs. (6.1) and (2.3), we know that  $\psi'_1(t)$  and  $\psi'_2(t)$  are bounded in  $[1, \infty)$ . Applying Lemma 4.1 to Eq. (6.3), we conclude that  $\psi_1(t), \psi_2(t) \rightarrow 0$  as  $t \rightarrow \infty$ . Therefore

$$\lim_{t \rightarrow \infty} \int_{\Omega} \{ |\nabla S|^2 + |\nabla I|^2 + |\nabla P|^2 \} dx = 0, \quad (6.5)$$

$$\lim_{t \rightarrow \infty} \int_{\Omega} (S - S^*)^2 dx = 0, \quad (6.6)$$

$$\lim_{t \rightarrow \infty} \int_{\Omega} (I - I^*)^2 dx = 0. \quad (6.7)$$

From (6.5) and the Poincare inequality, we deduce that

$$\lim_{t \rightarrow \infty} \int_{\Omega} (S - \bar{S})^2 + (I - \bar{I})^2 + (P - \bar{P})^2 dx = 0. \quad (6.8)$$

By definition  $\bar{f} := \frac{1}{|\Omega|} \int_{\Omega} f dx$  for a function  $f \in L^1(\Omega)$ . Now, using the third equation in (2.3), it follows from (6.8) that

$$\begin{aligned} |\Omega| \bar{P}(t) &= \frac{d}{dt} \int_{\Omega} P(t) dx \\ &= \omega_4 \int_{\Omega} P \left( \frac{S}{S + b_1 I + c_1} - \frac{S^*}{S^* + b_1 I^* + c_1} \right) dx \\ &\quad + \omega_3 \int_{\Omega} P \left( \frac{I}{S + b_1 I + c_1} - \frac{I^*}{S^* + b_1 I^* + c_1} \right) dx \rightarrow 0, \\ & \text{as } t \rightarrow \infty. \end{aligned} \quad (6.9)$$

Since  $\bar{S}(t) \rightarrow S^*$ ,  $\bar{I}(t) \rightarrow I^*$  and  $\bar{P}(t)$  is bounded, we infer that there exists a sequence  $\{t_m\}$  with  $t_m \rightarrow \infty$ ; and a positive constant  $\hat{P}$  such that

$$\bar{S}'\{t_m\} \rightarrow 0, \quad \bar{I}'\{t_m\} \rightarrow 0, \quad \text{and} \quad \bar{P}\{t_m\} \rightarrow \hat{P}. \quad (6.10)$$

At  $t = t_m$  we write

$$\begin{aligned}\bar{S}' &= \int_{\Omega} (S - S^*) \left[ r \left( 1 - \frac{S+I}{K} \right) - \frac{\beta I}{S+I+c} - \frac{\omega_1 P}{S+b_1 I + c_1} \right] dx \\ &\quad + \int_{\Omega} S^* \left[ r \left( 1 - \frac{S+I}{K} \right) - \frac{\beta I}{S+I+c} - \frac{\omega_1 P}{S+b_1 I + c_1} \right] dx, \quad (6.11)\end{aligned}$$

$$\begin{aligned}\bar{P}' &= \int_{\Omega} (I - I^*) \left[ \frac{\beta S}{S+I+c} - \frac{\omega_2 P}{S+b_1 I + c_1} - a \right] dx \\ &\quad + \int_{\Omega} I^* \left[ \frac{\beta S}{S+I+c} - \frac{\omega_2 P}{S+b_1 I + c_1} - a \right] dx. \quad (6.12)\end{aligned}$$

Applying (6.8) and (6.10), it follows from (6.11) that  $\hat{P} \neq 0$ ,  $r(1 - \frac{S+I}{K}) - \frac{\beta I}{S+I+c} - \frac{\omega_1 P}{S+b_1 I + c_1} = 0$  and  $\frac{\beta S}{S+I+c} - \frac{\omega_2 P}{S+b_1 I + c_1} - a = 0$  and hence  $\hat{P} = P^*$ . Consequently

$$\lim_{m \rightarrow \infty} \bar{S}(t_m) = S^*, \quad \lim_{m \rightarrow \infty} \bar{I}(t_m) = I^*, \quad \text{and} \quad \lim_{m \rightarrow \infty} \bar{P}(t_m) = P^*. \quad (6.13)$$

Since  $\|S(\cdot, t_m)\|_{C^{2,\alpha}(\bar{\Omega})} \leq C$ ,  $\|I(\cdot, t_m)\|_{C^{2,\alpha}(\bar{\Omega})} \leq C$  and  $\|P(\cdot, t_m)\|_{C^{2,\alpha}(\bar{\Omega})} \leq C$ , there exists a subsequence of  $\{t_m\}$ , still denoted by the same notation, and positive functions  $u_i \in C^2(\bar{\Omega})$ , such that

$$\begin{aligned}\lim_{m \rightarrow \infty} \|S(\cdot, t_m) - u_1(\cdot)\|_{C^2(\bar{\Omega})} &= 0, \quad \lim_{m \rightarrow \infty} \|I(\cdot, t_m) - u_2(\cdot)\|_{C^2(\bar{\Omega})} = 0, \\ \text{and} \quad \lim_{m \rightarrow \infty} \|P(\cdot, t_m) - u_3(\cdot)\|_{C^2(\bar{\Omega})} &= 0.\end{aligned}$$

In view of (6.13), we know that  $u_1^* \equiv S^*$ ,  $u_2^* \equiv I^*$  and  $u_3^* \equiv P^*$ . Therefore

$$\begin{aligned}\lim_{m \rightarrow \infty} \|S(\cdot, t_m) - S^*\|_{C^2(\bar{\Omega})} &= 0, \quad \lim_{m \rightarrow \infty} \|I(\cdot, t_m) - I^*\|_{C^2(\bar{\Omega})} = 0, \text{ and} \\ \lim_{m \rightarrow \infty} \|P(\cdot, t_m) - P^*\|_{C^2(\bar{\Omega})} &= 0. \quad (6.14)\end{aligned}$$

The global asymptotic stability of  $E^*$  follows from Eq. (6.14) and the local stability of  $E^*$ .

## References

- [1] R.M. Anderson, R.M. May, Population biology of infectious diseases: part i, *Nature* 280 (1979) 361–367.
- [2] J. Abrantes, W.V.D. Loo, J.L. Pendu, P.J. Esteves, Rabbit hemorrhagic disease (RHD) and rabbit haemorrhagic disease virus (RHDV): a review, *Vet. Res.* 43 (2012) 1–12.
- [3] N. Bairagi, D. Adak, Complex dynamics of a predator prey parasite system: an interplay among infection rate, predator's reproductive gain and preference, *Ecol. Complex.* 22 (2015) 1–12.
- [4] A.M. Bate, F.M. Hilker, Complex dynamics in an eco-epidemiological model, *Bull. Math. Biol.* 75 (2013) 2059–2078.
- [5] M. Branco, N. Ferrand, M. Monnerot, Phylogeography of the European rabbit (*Oryctolagus cuniculus*) in the iberian peninsula inferred from RFLP analysis of the cytochrome b gene, *Heredity* 85 (2000) 307–317.
- [6] F. Brauer, P. van den Driessche, J. Wu, *Mathematical Epidemiology*, Lecture Notes in Mathematics, Springer, 2008.
- [7] C. Calvete, Modeling the effect of population dynamics on the impact of rabbit hemorrhagic disease, *Conserv. Biol.* 20 (2006) 1232–1241.
- [8] T.J. Case, Illustrated guide to theoretical ecology, *Ecology* 80 (1999) 2848.
- [9] J. Chattopadhyay, O. Arino, A predator-prey model with disease in the prey, *Nonlinear Anal.* 36 (1999) 747–766.
- [10] J. Chattopadhyay, P.D.N. Srinivasu, N. Bairagi, Pelicans at risk in Salton Sea an eco-epidemiological model-II, *Ecol. Model.* 167 (2003) 199–211.
- [11] S. Chatterjee, D. Kesh, N. Bairagi, How population dynamics change in presence of migratory prey and predator's preference, *Ecol. Complex.* 11 (2012) 53–66.
- [12] K.P. Dalton, I. Nicieza, J. Abrantes, P.J. Esteves, F. Parra, Spread of new variant RHDV in domestic rabbits on the Iberian peninsula, *Vet. Microbiol.* 169 (2014) 67–73.
- [13] M. Delibes, A. Rodriguez, P. Ferreras, Action Plan for the Conservation of the Iberian Lynx in Europe (*Lynx pardinus*) in Europe, Nature and Environment Series, vol. 111, Council of Europe Publishing, 2000.
- [14] M. Delibes-Mateos, P. Ferreras, R. Villafuerte, European rabbit population trends and associated factors: a review of the situation in the Iberian peninsula, *Mamm. Rev.* 39 (2009) 124–140.
- [15] M. Delibes-Mateos, C. Ferreira, F. Carro, M.A. Escudero, C. Gortázar, Ecosystem effects of variant rabbit hemorrhagic disease virus, Iberian peninsula, *Emerg. Inf. Dis.* 20 (2014) 2166–2168.
- [16] O. Diekmann, J.A.P. Heesterbeek, J.A. Metz, On the definition and the computation of the basic reproduction ratio  $r_0$  in models for infectious diseases in heterogeneous populations, *J. Math. Biol.* 28 (1990) 365–382.
- [17] O. Diekmann, M. Kretzschmar, Patterns in the effects of infectious diseases on population growth, *J. Math. Biol.* 29 (1991) 539–570.
- [18] P. Ferreras, A. Travaini, S.C. Zapata, M. Delibes, Short-term responses of mammalian carnivores to a sudden collapse of rabbits in Mediterranean Spain, *Basic Appl. Ecol.* 12 (2011) 116–124.
- [19] D.A. Fordham, H.R. Akakaya, B.W. Brook, A. Rodriguez, P.C. Alves, E. Civantos, M.T. no, M.J. Watts, M.B. Arajo, Adapted conservation measures are required to save the Iberian lynx in a changing climate, *Nat. Clim. Chang.* 3 (2013) 899–903.
- [20] M.R. Garvie, Finite-difference schemes for reaction-diffusion equations modelling predator-prey interactions in MATLAB, *Bull. Math. Biol.* 69 (2007) 931–956.
- [21] S.R. Hall, M.A. Duffy, C.E. Cáceres, Selective predation and productivity jointly drive complex behavior in host-parasite systems, *Am. Nat.* 165 (2005) 70–81.
- [22] M. Haque, J. Chattopadhyay, Role of transmissible disease in an infected prey-dependent predator-prey system, *Math. Comput. Model. Dyn. Syst.* 13 (2007) 163–178.
- [23] M. Haque, E. Venturino, The role of transmissible diseases in the Holling-Tanner predator-prey model, *Theor. Popul. Biol.* 70 (2006) 273–288.
- [24] M. Haque, M.S. Rahman, E. Venturino, Comparing functional responses in predator-infected eco-epidemics models, *Biosystems* 114 (2013) 98–117.
- [25] H.W. Hethcote, W. Wang, L. Han, Z. Ma, A predator-prey model with infected prey, *Theor. Popul. Biol.* 66 (2004) 259–268.
- [26] F.M. Hilker, H. Malchow, Strange periodic attractors in a prey-predator system with infected prey, *Math. Popul. Stud.* 13 (2006) 119–134.
- [27] K.E. Hedges, C.J. Krebs, A.R.E. Sinclair, Snowshoe hare demography during a cyclic population low, *J. Anim. Ecol.* 68 (1999) 581–594.
- [28] Y.H. Hsieh, C.K. Hsiao, Predator-prey model with disease infection in both populations, *Math. Med. Biol.* 25 (2008) 247–266.
- [29] W.E. Johnson, J.A. Godoy, F. Palomares, M. Delibes, M. Fernandes, E. Revilla, S.J. O'Brien, Phylogenetic and phylogeographic analysis of Iberian lynx populations, *J. Hered.* 95 (2004) 19–28.
- [30] S.E. Jorgensen, *Handbook of Environmental Data and Ecological Parameters*, Pergamon Press, 1979.
- [31] E.J. Kormondy, *Concepts of Ecology*, Prentice-Hall, Inc., Englewood Cliffs, N. J., 1969.
- [32] A.A. King, W.M. Schaffer, The geometry of a population cycle: a mechanistic model of snowshoe hare demography, *Ecology* 82 (2001) 814–830.
- [33] O. Lakkis, A. Madzvamuse, C. Venkataraman, Implicit-explicit timestepping with finite element approximation of reaction-diffusion systems on evolving domains, *SIAM J. Numer. Anal.* 51 (2013) 2309–2330.
- [34] Y. Lv, R. Yuan, Y. Pei, Turing pattern formation in a three species model with generalist predator and cross-diffusion, *Nonlinear Anal. Theory Methods Appl.* 85 (2013) 214–232.
- [35] H. Malchow, S.V. Petrovskii, E. Venturino, *Spatiotemporal Patterns in Ecology and Epidemiology: Theory, Models, and Simulation*, Chapman and Hall/CRC Press, London, 2008.
- [36] H. McCallum, N. Barlow, J. Hone, How should pathogen transmission be modelled? *Trends Ecol. Evol.* 16 (2001) 295–300.
- [37] A. Okubo, S.A. Levin, *The basics of diffusion, Diffusion and Ecological Problems: Modern Perspectives*, Springer, New York, 2001.
- [38] M. Otero, H.G. Solari, Stochastic eco-epidemiological model of dengue disease transmission by aedes aegypti mosquito, *Math. Biosci.* 223 (2010) 32–46.
- [39] F. Palomares, A. Rodriguez, E. Revilla, J.V. López-Bao, J. Calzada, Assessment of the conservation efforts to prevent extinction of the Iberian lynx, *Conserv. Bio.* 25 (2011) 4–8.
- [40] M. Pascual, Diffusion-induced chaos in a spatial predator-prey system, *Proc. R. Soc. Lond. Ser. B Biol. Sci.* 251 (1993) 1–7.
- [41] S.V. Petrovskii, H. Malchow, Wave of chaos: new mechanism of pattern formation in spatiotemporal population dynamics, *Theor. Popul. Biol.* 59 (2001) 157–174.
- [42] R. Real, A.M. Barbosa, A. Rodriguez, F.J. Garca, J.M. Vargas, L.J. Palomo, M. Delibes, Conservation biogeography of ecologically interacting species: the case of the Iberian lynx and the European rabbit, *Divers. Distrib.* 15 (2009) 390–400.
- [43] B. Reddiex, G.J. Hickling, G.L. Norbury, C.M. Frampton, Effects of predation and rabbit haemorrhagic disease on population dynamics of rabbits (*Oryctolagus cuniculus*) in north canterbury, *Wildl. Res.* 29 (2003) 627–633.
- [44] A. Rodriguez, M. Delibes, Internal structure and patterns of contraction in the geographic range of the Iberian lynx, *Ecoigraphy* 25 (2002) 314–328.
- [45] A. Rodriguez, M. Delibes, Patterns and causes of non-natural mortality in the Iberian lynx during a 40-year period of range contraction, *Biol. Conserv.* 118 (2004) 151–161.
- [46] P. Roy, R.K. Upadhyay, Conserving Iberian lynx in Europe: issues and challenges, *Ecol. Complex.* 22 (2015) 16–31.
- [47] L.F. Ruggiero, K.B. Aubry, S.W. Buskirk, G.M. Koehler, C.J. Krebs, K.S. McKelvey, J.R. Squires, *Ecology and Conservation of Lynx in the United States*, Univ. Press of Colorado, USA, 1999. USDA Rocky Mountain Research Station.
- [48] J. Sotomayor, Generic bifurcations of dynamical systems, *Dyn. Syst.* (1973) 561–582.
- [49] D. Stiefsa, E. Venturino, U. Feudel, Evidence of chaos in eco-epidemic models, *Math. Biosci. Eng.* 6 (2009) 855–871.

- [50] D.P. Tittensor, M. Walpole, S.L.L. Hill, et al., A mid-term analysis of progress toward international biodiversity targets, *Science* 346 (2014) 2417–244.
- [51] R.K. Upadhyay, S.R.K. Iyengar, *Introduction to Mathematical Modeling and Chaotic Dynamics*, CRC Press, 2013.
- [52] R.K. Upadhyay, N. Bairagi, K. Kundu, J. Chattopadhyay, Chaos in eco epidemiological problem of the Salton sea and its possible control, *Appl. Math. Comput.* 196 (2008) 392–401.
- [53] M. Wang, *Nonlinear Partial Differential Equations of Parabolic Type*, Science Press, Beijing, 1993.
- [54] P.J. White, R.C. Trout, S.R. Moss, A. Desai, M. Armesto, N.L. Forrester, P.J. Hudson, et al., Epidemiology of rabbit haemorrhagic disease virus in the united kingdom: evidence for seasonal transmission by both virulent and avirulent modes of infection, *Epidemiol. Infect.* 132 (2004) 555–567.
- [55] Y. Xiao, L. Chen, Analysis of a three species eco-epidemiological model, *J. Math. Anal. Appl.* 258 (2001) 733–754.